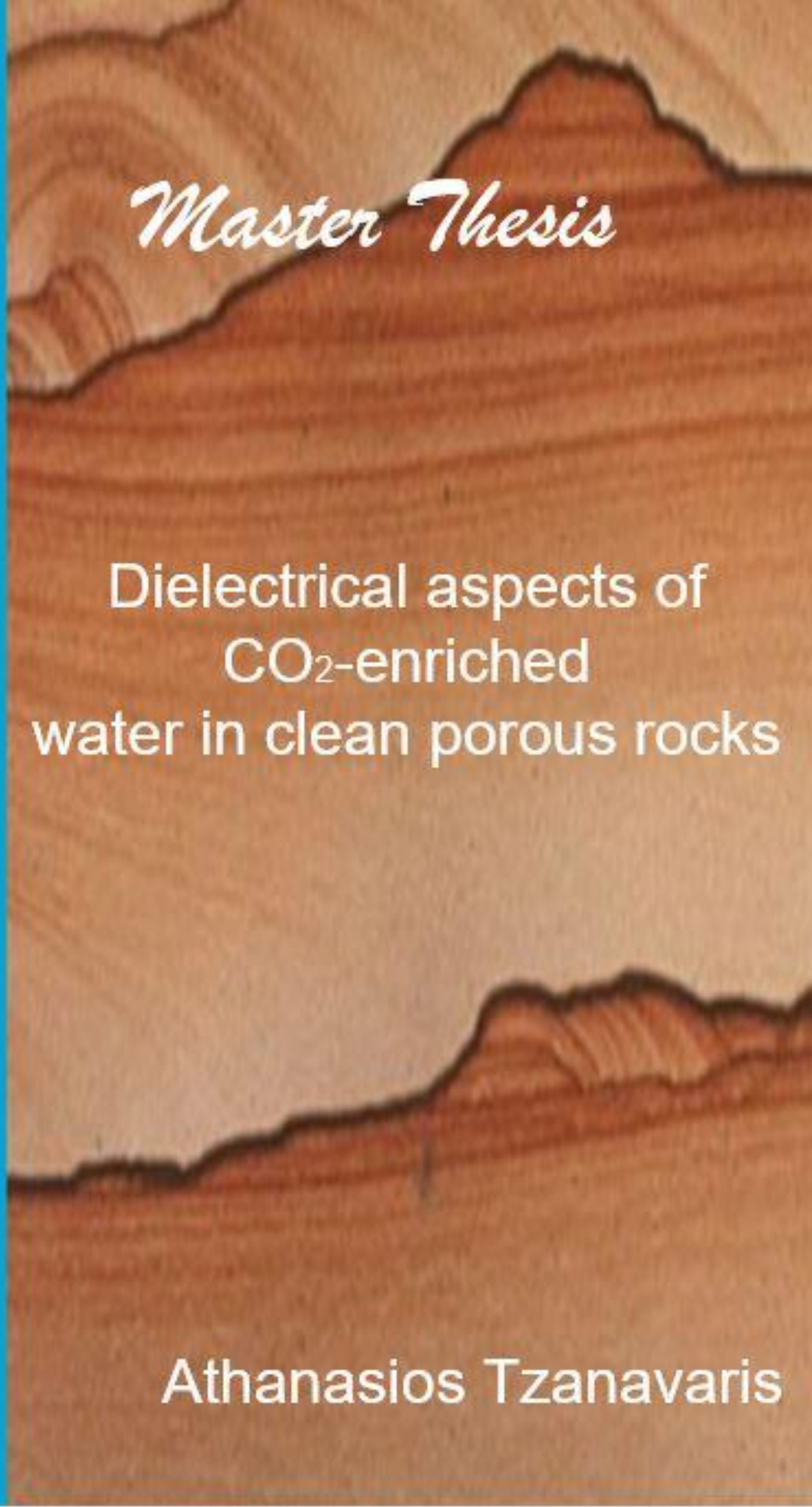

Master Thesis

Dielectrical aspects of CO_2-enriched water in clean porous rocks

TU Delft

Athanasios Tzanavaris

Dielectrical aspects of CO_2-enriched water in clean porous rocks

(D.A.C.E.W.C.P.R.)

Experimental and modeling study

by

Athanasios Tzanavaris

in partial fulfilment of the requirements for the degree of

Master of Science
in Applied Earth Science

at Delft University of Technology
to be publicly defended on Monday October 10, 2016 at 16:30 PM.

Professor:
Prof. Dr. Pacelli L.J. Zitha — Delft University of Technology

Supervisor:
Dr. Karl-Heinz A. A. Wolf — Delft University of Technology

Thesis committee members:
Prof. Dr. J. (Hans) Bruining — Delft University of Technology
Prof. Dr. Ir. Evert C. Slob — Delft University of Technology
Dr. Claire Chassagne — Delft University of Technology
Mr. Faisal Al Saadi — Shell Global Solutions B.V.

Dielectrical aspects of CO_2-enriched water in clean porous rocks

Athanasios Tzanavaris[1], Karl-Heinz A. A. Wolf[2], Pacelli L.J. Zitha[3]

Abstract

Streaming potential is an eletrokinetic effect which reflects the electrical charge or the electrical potential created by flow of ionic fluids through porous media, such as hydrocarbon reservoir rocks. The concept has been studied mostly for low salinity fluids and in the past decade consist a subject of interest in oil & gas industry. Dielectric studies concerning different ionic fluids used in enhance oil recovery (EOR) are limited.

In this study we investigate if available models for low salinity fluids can be modified and redeveloped to describe the behavior of streaming potential coefficient and zeta potential for carbonated water flooding in reservoir rocks with very small clay content. The model presented in this work follows the approach of Glover et al. published in 2012. The developed theoretical model suggested here is sensitive to salinity, temperature, reservoir rock properties and fluid properties, while the main variable is pore fluid concentration.

For the verification of the theoretical estimations, core flooding experiments were performed with different CO_2-enriched solutions in Fontainebleau sandstone sample. From comparison of the experimental measurements with the theoretical estimations, it was observed that the model can produce estimations of ζ potential and streaming potential coefficient (C_S) as a function of pore fluid concentration within a *pH* range of 4 to 7. Moreover, it was observed that for the correlation a coefficient introduced by Glover et al. in 2012 had to be implemented.

Keywords

CO_2, Carbonated Water, Fontainebleau, CWI, Zeta potential, Streaming potential coefficient

[1]Department of Petroleum Engineering and Geoscience, Delft University of Technology, Netherlands
[2]Department of Petroleum Engineering and Geoscience, Delft University of Technology, Netherlands
[3]Department of Petroleum Engineering and Geoscience, Delft University of Technology, Netherlands

1 Introduction

Multiple studies during the past years have addressed eletrokinetic properties of porous media aiming to improve our understanding of electrokinetics. Electrokinetics is a general term associated with the relative motion between two or more charged phases [1]. When there is a tangential movement of phases across boundaries of surface-liquid or liquid-gas or solid-gas phases, a number of electrokinetic phenomena can occur [2]. Those electrokinetic phenomena can be characterized as electrokinetic effects. Among those, the most common are electrophoresis, electro-osmosis, streaming potential (C_s), and sedimentation potential.

Monitoring of electrokinetic effects generated in the subsurface have a wide range of applications in oil and gas reservoir modeling, aquifer depletion, geothermal energy [3], forecast of volcanic activity and earthquake prediction [4]. In the oil and gas industry, downhole installations were designed to measure electrokinetic effects have been reported. Those measurements, may be used as an indicator for the nature of hydraulic transfers in very heterogeneous reservoirs [5] and consequently with further equipment, such as smart wells, may influence the production rate by changing the fluid flow of the well remotely [6] or improve enhance oil recovery (EOR) methods, such as waterflood by the modification of injection brine ionic composition [7].

The streaming potential is the electric potential that is generated when an electrolyte fluid flows through a stationary charged solid, such as porous media, by an applied pressure gradient [1,2,8]. It occurs within the electric double layer (EDL), which is a concept that was introduced by Helmholtz and was deliberated by Stern, as discussed in appendix A. According to Saunders et al. [9], its value depends on the electrolyte concentration, electrolyte pH, ionic species within the electrolyte fluid, temperature, rock mineralogy, and rock structure at a given pressure. Helmholtz and Smoluchowski quantified streaming potential *(C_S)* in capillary tubes and they developed an equation knows as HS equation given as:

$$C_s = \frac{\Delta V}{\Delta P} = \frac{\varepsilon_r \varepsilon_o \zeta}{\eta_f \sigma_f}, \qquad (1)$$

Here, C_s (V/Pa) stands for streaming potential coupling co-efficient and is the ratio of ΔV (V) the measured streaming potential to ΔP (Pa) the applied fluid pressure difference that drives the fluid through the capillary tube; ε_r is the relative permittivity of the pore fluid; ε_o is the electric permittivity of free space (≈8.854 10 – 12 F/m); η_f is the dynamic viscosity of the pore fluid (Pa.s); ζ refers to zeta potential and σ_f represents the pore fluid electrical conductivity [10].

HS equation is accepted by the scientific community as a formula that can be applied in any porous medium including reservoir rocks. It is commonly used for the estimation of the zeta potential (ζ), the potential in the Stern layer of EDL, or other petrophysical properties of reservoir rocks, under the assumption that the ratio of pore radius and Debye length is relative large such that no overlap occurs in the EDL [10]. When this is not the case, additional parameters influence fluid conductivity and the formula should be written as [11, 12, 10]:

$$C_s = \frac{\Delta V}{\Delta P} = \frac{\varepsilon_r \varepsilon_o \zeta}{\eta_f \left(\sigma_f + \frac{2\Sigma_s}{\Lambda}\right)}, \quad (2)$$

Where, Σ_s refers to the specific surface conductance and Λ is a length scale characteristic of the pore microstructure (Λ=d/(3(F-1))) [13, 11], for which a detail discussion can be found in Revil et. al. [4]. Further modifications in streaming potential formula, mentioned above, have been published by Glover et al. [11] in 2010. They develop two formulas that link the streaming potential coefficient (C_s) to the zeta potential (ζ) with respect to the mean pore radius and the mean grain diameter respectively, which yield:

$$C_s = \frac{\Delta V}{\Delta P} = \frac{r \varepsilon_r \varepsilon_o \zeta}{\eta_f (r\sigma_f + 2\Sigma_s\sqrt{3})}, \quad (3)$$

$$C_s = \frac{\Delta V}{\Delta P} = \frac{\varepsilon_r \varepsilon_o \zeta}{\eta_f (d\sigma_f + 6\Sigma_s(F-1))} \quad (4)$$

where, Σ_s (S) refers to the specific surface conductance and Λ (m). In equation 3, r is the mean pore radius and $\varepsilon_f = \varepsilon_r\varepsilon_o$, while in equation 4, d is the mean grain diameter and F is the formation factor, obtained usually by Archie's equation which can be found in appendix B.

The above equations have been extensively used in research studies, such as Glover et al. [14] or Werner et al. [15], for the description and modeling of zeta potential and streaming potential dependency on pore fluid salinity changes. Essentially, they investigate how a theoretical model can accurately describe those two electrokinetic effects, streaming potential and ζ potential, generated by the interaction between different reservoir rocks, usually with composition rich in silicates (quartz) (SiO_2) and poor in alominosilicates (clay) (Al), and electrolyte solutions with different NaCl concentrations. Despite, the variety in ionic fluids, the available models are limited only in the interaction of mineral and NaCl variation. Schramm et al. [16] though, states that the sensitivity of minerals to small changes in electrolyte properties, carries potentially serious implications for any injection process whose efficiency depends indirectly on surface charge. Thus, one may say that any fluid used in EOR with high ionic concentration can become a source that may generate those electrokinetic effects when it flows through a reservoir rock.

Carbonated water (CW) (or CO2-enriched water) consists of such a fluid used in carbonated water injection (CWI), an alternative CO_2 injection strategy, where CO_2 exist as a dissolved phase into the solution [17] with the chemical formula: $H_2O + CO_2 \leftrightarrow HCO_3^- + H^+$. CWI is characterized as an improved water flooding technique and a very promising EOR process [18]. The reason is that the mixture benefits from both water and CO_2 properties, resulting to a better sweep efficiency, lower mobility which retards the breakthrough time of CO_2 and reduces oil swelling effect [19, 20]. It is also considered to be one of the safer ways for CO_2 storage because reduces the risk of leakage of CO_2 through caprock [17].

The scope of this paper is to investigate whether the existing theoretical models available are valid under modifications for streaming potential and zeta potential during CW flooding, to provide a model that may be used for future research regarding CWI and examine if the developed model can be applied in reservoir rocks with small clay content. To validate this theoretical approach a single reservoir rock type has been selected for laboratory experiments, named Fontainebleau sandstone (SST). This sandstone has been extensively studied which is beneficial because a wide range of information are accessible in the literature (e.g., Mijtterlose et al. [21], Mutterlose et al. [22], Thiry et al. [23], Cooper et al. [24]), have been used in similar experimental work and they consists ideal an sample for this research topic because of its composition.

Fontainebleau is a quartz rich homogeneous SST containing typically more than 98% of quartz [25] and is well sorted with average grain size around 250 μm [26] and porosity that varies between 2 and 30%. It has been interpreted as a Stampian age (early Oligocene) sandstone [23] and according to Coker et al. [27] may be treated as a two-phase material consisting of grains (quartz) and porosity.

From literature review, we found that the most suitable theoretical approach for this research topic is Glover et al. [14] published in 2012, developed with respect to equation 4. This selection has been made manly because of the majority of the parameters in this publication are based on empirical correlations. Both the model and correlations have been corrected and modified to account for the two SST properties under different CW consecration flooding. Before the fluid modifications were applied, a base case scenario was created for the confirmation that the theoretical model can reflect the properties of this particular reservoir sandstone. Finally, the experimental results are compared with the theoretical estimations to validate our hypothesis which concerns the following:

- investigation whether the available theoretical model is valid under modifications for CW flooding.
- examine if the developed model can be applied in reservoir rocks with small clay content.
- provide a model that may be used in further research

2 Theoretical model and parameter definition

As was mentioned previously, the theoretical model presented in this paper follows the same principals and methods of the model indicated by Glover et al. [14] in 2012 (Figure 1). It is developed based on the equation 4. Before any modification was applied, their model was revised and its parameters were corrected according to the corresponding literature sources. The modifications ware mainly on fluid properties and their corresponding formulas, while formulas regarding rock properties remain untouched. More specifically, two empirical correlations have been implemented for the estimation of the equilibrium dissociation constants pK_1 and pK_2, an additional formula has been suggested for the determination of CW pore fluid conductivity (σ_f). So, the values of the remaining fluid properties have been altered to be suitable with the CW solution. Moreover, the changes were defined such that the modified theoretical model can provide estimations within the range of 0°C ≤ T ≤ 100 °C and 5 bar ≤ P ≤ 65 bar. These are conditions that were satisfied also from the initial model.

A detailed discussion for the formulas used to define the parameters of equation 4 and model the behavior of the zeta potential and streaming potential as a function of pore fluid concentration is explained bellow. The associated input parameters of the modified theoretical model, and rock properties of the Fontainebleau sandstone sample, and fluid properties, are given in Table 1. Note that the sensitivity of the parameters in the theoretical model is not included in this paper.

2.1 Pore fluid electric permittivity (ε_f)

$$\varepsilon_f = \varepsilon_r \varepsilon_o \tag{5}$$

The value of pore fluid electric permittivity (ε_f) depends upon relative electric permittivity (ε_r) and the electric permittivity in vacuo (ε_o), indicated in equation 5. While electric permittivity in vacuo has a constant value of ε_o = 8.854 x 10^{-12} F/m, relative electric permittivity varies with environmental conditions. Gary Olhoeft implied that temperature and fluid pH have a significant impact on relative permittivity ε_r value. Thus, he developed an empirical equation to include those effects (equation 5), which can be written as:

$$\varepsilon_r(T, C_f) = a_0 + a_1 T + a_2 T^2 + a_3 T^3 + c_1 C_f + c_2 C_f^2 + c3 C_f^3, \tag{6}$$

Here, α_0 = 295.68, α_1 = -1.2283 (K^{-1}), α_2 = 2.094 x 10^{-3} (K^{-2}), α_3 = -1.41 x 10^{-6} (K^{-3}), c_1 = -13.00 ($Lmole^{-1}$), c_2 = 1.065 $(Lmole^{-1})^2$, c_3 = -0.03006 $(Lmole^{-1})^3$, T (K) is the temperature, and C_f (mol/L) expresses the bulk pore fluid salinity. Note that, this formula is valid for temperatures within the magnitude of 273 < T <373(K).

2.2 Fluid dynamic viscosity (η_f)

According to Glover et al. [14], dynamic viscosity of pore fluid (η_f) can be estimated by the empirical equation of Phillips et al. [29] which is defined as:

$$\eta_f(T, C_f) = e_1 + e_2 \exp(a_1 T) + e_3 \exp(a_2 C_f^m) + e_4 \exp(a_3 T + a_4 C_f^m), \tag{7}$$

where, e_1 = 4.95166 x 10^{-5} (Pa.s), e_2 = 6.034658 x 10^{-4} (Pa.s), e_3 = 9.703832 x 10^{-5} (Pa.s), e_4 =1.025107 x 10^{-3} (Pa.s), α_1 = -0.06653081/°C, α_2 = 0.1447269/mol, α_3= -0.02062455/°C, α_4 = 0.1301095/mol, T (°C) is the temperature and C_f^m is the molality of the bulk pore fluid.

This equation is valid for both strong and weak solutions. For weak fluid solutions the molality is equal to $C_f^m = C_f$. For strong solutions it is equal to $C_f^m = \mathrm{C_f} / (\rho_f - (\mathrm{AC_f}/1000))$, where ($\rho_f$ (g/cm3) is the fluid density and A (g/mol) is the atomic weight of sault [14]. In this research topic CW is considered to be a weak solution.

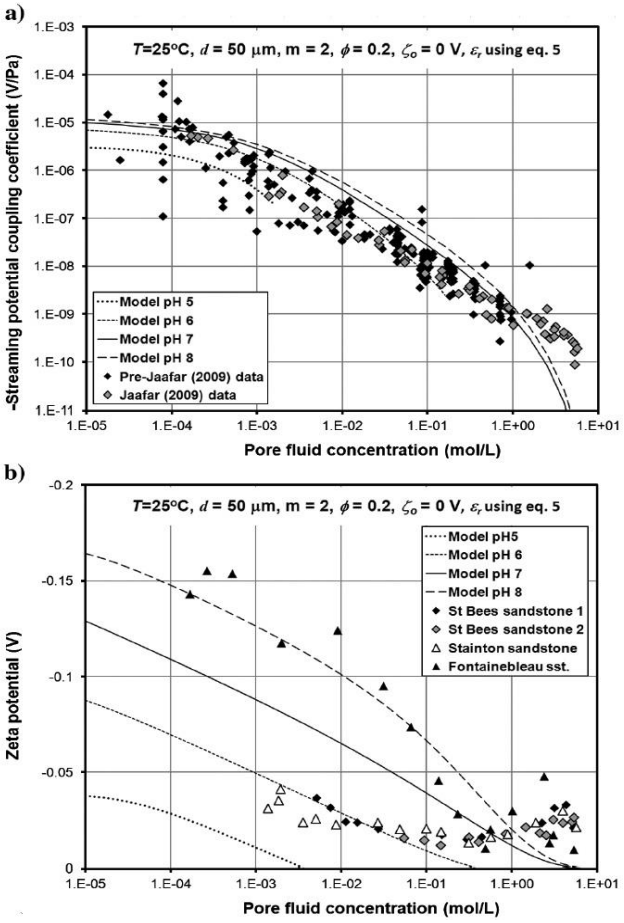

Figure 1. Models and experimental measrements of streaming potential coefficient and zeta potential as a function of pore fluid (NaCl) concentration for different pH values (from Glover et al. [14]). (a) Theoretical modeling of streaming potential coefficient for experimental data sets. (b) Theoretical modeling of zeta potential for the same and additional data sets obtained from the literature.

2.3 Debye length (χ_d)

Debye length is a parameter that expresses the distance between the Stern layer and the plane of shear within the diffuse part of EDL. Thus, it can be said that, Debye length describes the distance where the electrostatic effects are still

present during the interaction of a solid and a solution. It is defined as [30]:

$$\frac{1}{\chi_d^2} = \sum_{n}^{i=1} \frac{(ez_i)^2 N C_f}{\varepsilon_o \varepsilon_r k_b T}, \quad (8)$$

where, k_b = 1.38 x 10^{-23} (JK^{-1}) is the Boltzmann's constant, e = 1.602 x 10^{-19} (°C) express the elementary charge, N = 6.022 x 10^{23} (mol^{-1}) is Avogadro's constant, z_i refers to ionic species and If is the ionic strength [30]. In this research the dominant component of the fluid is CO_2 and thus it is assumed that z_i is unity. The formula of ionic strength yields:

$$I_f = \frac{1}{2}\sum_{i}^{n} z_i^2 C_i^f, \quad (9)$$

By combining equation 8 and equation 9, equation 8 can be written as:

$$\chi_d = \sqrt{\frac{\varepsilon_o \varepsilon_r k_b T}{2000 N e^2 I_f}} \quad (10)$$

where, 2000 is a correction factor used since the units of ionic strength are in mol/L. Glover et al. [14] imply that for concentrations greater than 10^{-5} mol/L and pH more than pH_{pzc}, ionic strength is considered to be $I_f \approx C_f$. Here this is not the case, thus the ionic strength has been estimated based on the equation 9.

2.4 Fluid pH

The possible amount of dissolved CO_2 in water is strongly related to the pH of the solution. McMahon et al. [31] pointed out that the most important parameters affecting dissolution of CO_2 are temperature, pressure and water salinity. It is important to note that, when water salinity increases solubility decreases [28]. The equilibrium chemical reactions taking place when CO_2 dissolves into water are:

$$H_2O + CO_2 \leftrightarrow H_2CO_3 \quad (11)$$

which is an unstable fluid, and converts to the equilibrium relations:

$$H_2CO_3 \overset{K_1}{\leftrightarrow} HCO_3^- + H^+ \quad (12)$$

and

$$HCO_3^- \overset{K_2}{\leftrightarrow} CO_2^{3-} + H^+ \quad (13)$$

The two equilibrium dissociation constants for carbonic acid K_1 and K_2 can be calculated from the equation 14 and equation 15. A detailed description can be found in Millero et al. 2002 [32]. Those two equations (eq. 14,15) considered to produce estimations within the temperatures of 0 °C ≤ T ≤ 40 °C.

$$pK_1 = -8.712 - 9.460 \times 10^{-3} S + 8.56 \times 10^{-5} S^2 + 1355.1/T + 1.7976 \ln(T), \quad (14)$$

$$pK_2 = 17.0001 - 0.01259 S - 7.9334 \times 10^{-5} S^2 + 936.291/T - 1.87354 \ln(T) - 2.61471 S/T + 0.07479 S^2/T, \quad (15)$$

here, T is the temperature in K and S is the salinity of the solution. We are using these equations under the assumption that are valid for S=0, because the selected water of the operation fluid in the laboratory experiments is demineralized with almost zero salinity. Essentially, for a temperature of 30 °C, we obtain K_1=$10^{-6.0313}$ and K_2=$10^{-9.385}$, which were kept as constants for the theoretical modeling. Another factor that that varies with temperature and affects the pH of this SiO_2-H_2O-CO_2 system, is the water dissociation constant (Kw). The polynomial suggested by Glover et al. [14] delivers values for Kw in the range of 0 °C ≤ T ≤ 100 °C and is given as:

$$K_w = 6.9978 \times 10^{-16} + 5.0178 \times 10^{-16} T - 2.4434 \times 10^{-17} T^2 + 7.1948 \times 10^{-19} T^3, \quad (16)$$

where, T refers to the temperature, here defined in °C. Finally, we calculated the system pH using the cubic equation [14]:

$$C_{H+}^3 - (C_a - C_b) C_{H+}^2 - (K_w + K_1) C_{H+} - 2K_1 K_2 = 0 \quad (17)$$

where, C_a and C_b refer to the acid concentration and base concentration in mol/L. In this research, CO_2 is considered to be an acid and H_2O is treated as base. In the theoretical model, we assume that the system *pH* increases by addition of CO_2 into the water. The above equation can be solved by the Targlia-Cardano approach, which is explained in appendix C. Glover et al. [14] give two ways to link acid concentration, base concentration and *pH*. In this study, we use the one, where *pH* is defined as $pH = -\log_{10}(C_H^+)$ (definition of C_H^+ in equation 17), which will return the concentrations of C_a and C_b.

2.5 Pore fluid electrical conductivity (σ_f)

The electrical conductivity of carbonated rich solutions is expected to be significantly lower compared to the electrical conductivity of solutions containing NaCl. In the model of Glover et al. [14] the electrical conductivity is calculated as a function of temperature T and ionic concentration C_f by the empirical equation of Sen and Goode [33]. Similarly, we calculated σ_f (S/m) for this H_2O - CO_2 system as a function of T and C_f using the data published by Light et al. 1995 [34] (Figure 2) giving the σ_f - C_f relation:

$$\sigma_f(T, C_f) = 0.001 \times C_f^{0.4893} \quad (18)$$

Here, C_f is defined in mol/l. It should be noted that this equation is only valid for a temperature of T=30 °C. For σ_f calculations within the temperature range of 0°C ≤ T ≤ 100°C, similar equations can be obtained from Table 2 of Light et al. 1995 [34].

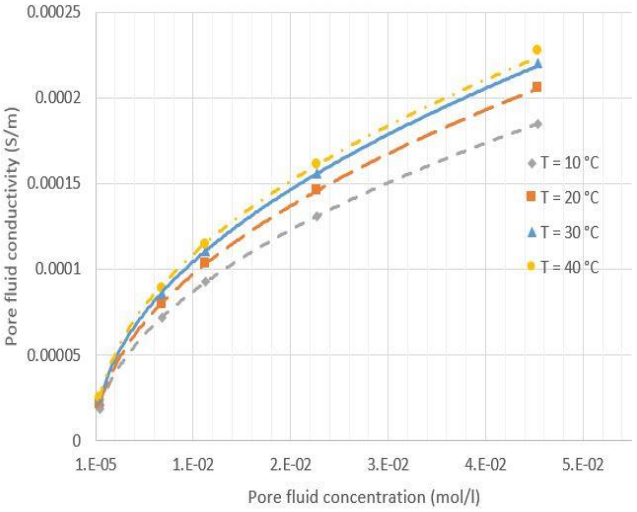

Figure 2. Conductivity values as a function of pore fluid ionic concentration for different temperatures obtained from Light et al. [34].

2.6 Pre-defined parameters

The fixed parameters with their corresponding values can be found in Table 1. The values of these parameters vary with properties of rock, fluid, temperature, etc. In this research they are considered to be constants. These parameters below, affect the values of surface condition (Σ_s) and Stern-plane potential (φ_d), which are discussed in sections 2.7 and 2.8 respectively.

Surface site density (Γ_s)

Lefevre et al. [35], at their publication in 2004, state that the surface site density (Γ_s) can be defined as the maximum surface density available for protonation or deprotonation, acidity constant, or electrostatic parameter. In the literature, the most common value reported for silica systems is Γ_s = 8nm^{-2} [36]. The value used in this theoretical model is Γ_s = 8.34nm^{-2} (Lofts et al. [37]), which is slightly smaller than the value of Γ_s =10nm^{-2} in Glover's model [11] (which reflects to NaCl full saturated measurements). In addition, we assume that no silica gel formation occurs; a phenomenon which will increase the value of Γ_s [4].

Disassociation constant for dehydrogenation ($pK\_$)

As was reported by Glover et al. [11] and Revil et al [4] the values that represent the disassociation constant for silica dehydrogenation is not yet well known. The most common values presented or used for research are within the range of 6.3 ≤ $pK\_$ ≤ 8.53 [38, 4, 39]. In this model we define $pK\_$ = 6.9, `because is a value compatible with the rest of the parameters (mainly with the temperature of T=30 °C).

Binding constant for cation adsorption (pK_{me})

Similarly with the value of pK_{me}, the value of binding constant for cation (carbon) adsorption of quartz is not yet well known [11, 4]. Experimental studies, from Su et al. [40] and Leckie et al. [41], show that the range of values for pK_{me} is fluctuating between 2.65 ≤ pK_{me} ≤ 7.9. In this model we define pK_{me}=7.1, a value slightly lower compared to the one in Glover's model. The value is close to the maximum value of CO_2 adsorption of quartz [40].

Surface ionic mobility (β_s)

For surface mobility (β_s) we are use the value of β_s = 5 x 10^{-9} (m^2/(Vs)) from Glover et al. [14] (smaller than the mobility of CO_2, β_s = 7.44 x 10^{-8} reported by Li et al. [42]). The reason is that the model is insensitive to small surface mobility variations for values less than 10^{-5}.

Proton conduction (Σ_s^{prot})

Proton conduction (Σ_s^{prot}) is one of the three parameters for surface conduction (Σ_s). It will be discussed in section 2.7. Glover et al. [14] defines the value of proton conduction as $\Sigma_s^{prot} = \Gamma_s \times c_{prot}$, where c_{prot} is a constant value obtained experimentally from Watillon and Backer [43] (1970). We define the proton conduction value directly, mainly for simplicity, as Σ_s^{prot} = 3.56 x 10^{-8} (S). This value has been obtained by extrapolation of the data presented in the work of Al-amsyar [44].

Shear plane distance (χ_ζ)

Surface of shear or shear plane, shown in Figure 3, is an imaginary surface close to the solid [2] and in between the Stern layer and the diffuse layer. The ions located in between the charged surface and Stern layer are immobile thus, the electric potential charges are zero. However, the ions that are located beyond the Stern plane form the diffuse mobile part, a part with an inner and an outer boundary, of the EDL [1]. The inner boundary of this mobile part called surface of shear and χ_ζ describes its distance from the surface.

There is no literature available concerning the shear plane distance of silica and a CO_2-enriched solution. There are two options that are suggested as possible solutions. The first option is the assumption that χ_ζ =0, (Borkovec et al [45] and Revil et al. [4]). The second option is to assume that the values in the literature for silica measured in low concentrations of NaCl, are valid for silica and CW. Consequently χ_ζ =2.4 x 10^{-10} (m), from Glover et al. [14], can be assigned. In this model we choose the second option to create a variation in the final streaming and zeta potential estimations.

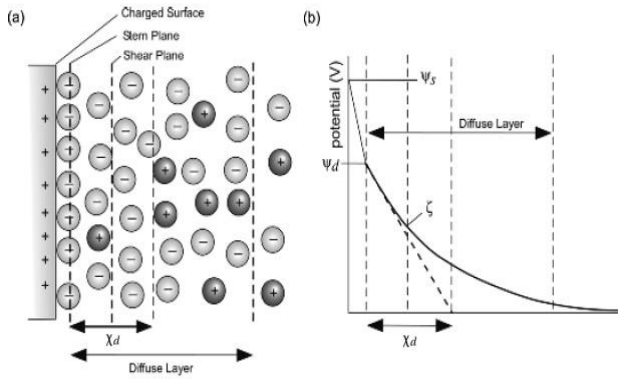

Figure 3. a) Schematic representation of the electric double layer according to the Stern model. (b) Schematic representation of the electric potential profile showing the Debye length (χ_d) and the overall extent of the electric double layer. The diffuse double layer starts from the Stern plane (from Masliyah et al. [1]).

2.7 Surface conduction (Σ_s)

For the calculation of the surface conduction (Σ_s), we follow the approach of Glover and Dery [11] instead of Glover et al. [14]. The reason is that Glover and Dery [11, 46] reduce the additional parameters by considering the conduction in the diffuse layer (Σ_s^{EDL}) as negligible. One of the parameters of the surface conduction (equation 19) is given as:

$$\Sigma_s = \Sigma_s^{EDL} + \Sigma_S^{Stern} + \Sigma_s^{prot} \tag{19}$$

In the equation 19, Σ_s^{stern} refers to conduction in the stern layer, calculated as [11]:

$$\Sigma_s^{stern} = \frac{e\beta_s \Gamma_s K_{Me} C_f}{(10^{-pH} + K_{\_}\left(\frac{\sqrt{8\times10^3 \varepsilon_f k_b N T}}{2e\Gamma_s K_{\_}} C^*\right)^{\frac{2}{3}} + K_{me} C_f}, \tag{20}$$

where, C^* was reported as [11]:

$$C^* = \left(\left(10^{-pH} K_{Me} C_f\right) \frac{\left(C_a + C_f + 10^{-pH}\right)}{\sqrt{I_f}}\right). \tag{21}$$

The dominant parameter that affects the surface conduction calculation is Σ_s^{prot}. The values of Σ_s, are based on the input parameters of this research and are within the magnitude of $3.56\text{x } 10^{-8} \leq \Sigma_s \leq 4.36\text{x}10^{-8}$ (S), for a concentration range of $10^{-5} \leq C_f \leq 10$ (mol/L) and T= 30 °C.

`

2.8 Stern plane potential (φ_d)

Up to this point it was discussed that the stern layer is located close to the surface of the solid (Figure 3), and that distance can be derived by the equation 10. Now the last component missing for the theoretical determination of ζ potential, is the value of the potential difference in the Stern layer (φ_d). Revil et al. [4] introduce a formula for the calculation of Stern layer (φ_d), which was used later by Glover and Dery [11], and is given as:

$$\varphi_d = \frac{2k_b T}{3e} \ln\left(\frac{\sqrt{8\times10^3 \varepsilon_f N T}\left(10^{-pH} + K_{me} C_f\right)}{2e\Gamma_s K_{\_}} \left(\frac{10^{-pH} C_f}{\sqrt{I_f}}\right)\right), \tag{22}$$

Here, ε_f refers to fluid electrical permittivity calculated by the equation 6 in (F/m); e=1.602 x 10^{-19}(C), k_b=1.38 x 10^{-23} (J/K) and N=6.022 x 10^{-23} (mol^{-1}) are the elementary charge, Boltzmann's constant and Avogadro's constant respectively; T is the temperature in K; I_f (mol/L) represents the ionic strength calculated by equation 9; C_f represents the ionic fluid concentration in mol/L; C_a refers to the acid consecration in mol/L; K_{Me} and $K_{\_}$ are the binding constant for cation adsorption on silica and the dissociation constant for dehydrogenization on silica respectively.

2.9 Zeta potential (ζ)

The zeta potential stands as the electrical potential, formed by any electrokinetic phenomenon, at the shear plane of the EDL. It has been noted that the distribution of the potential within the EDL has an exponential behavior [46, 14, 47] and can be calculated based on the linearized Poisson-Boltzmann equation, defined as:

$$\varphi = \varphi_d \exp(\chi/\chi_d) \tag{23}$$

where, χ is the distance from the mineral surface.

In addition, ζ is also generated within the EDL and by that is expected to have a similar exponential behavior in its distribution. According to Glover et al. [14], ζ potential should be calculated by the Debye-Huckel approximation, which yields:

$$\zeta = \varphi_d \ \exp(-\chi_\zeta/\chi_d) \tag{24}$$

where, φ_d (V) refers to stern plane potential calculated by equation 22, χ_ζ =2.4 x 10^{-10} (m) (the shear plane distance), and χ_d represents the Debye length calculated by the equation 10.

Table 1. Parameters of Fontainebleau SST used in the theoretical modeling of zeta potential (ζ) and further streaming potential coefficient (C_s), as were discussed previously. (Note that those parameter were defined to be compatible with the experimental conditions.)

		Fontainebleau SST	
Parameter	**Symbol**	**Value**	**Unit**
Environmental Conditions			
Temperature	T	30	°C
Rock properties			
Porosity	φ	0.12	(-)
Cementation factor	m	2	(-)
Formation factor*	F	69.44	(-)
Grain diameter	d	2.5×10^{-4}	(m)
Permeability**	k	16.09 ± 1.43	(mD)
Pore fluid properties			
Ionic concentration	C_f	10^{-5} to 10	(mol/l)
pH	pH	4 to 7	(-)
Dissociation constant	K_w	calculate from equation 16	(-)
Equilibrium dissociation constant of CO_2 in water	pK_1	calculate from equation 14	(-)
Equilibrium dissociation constant of carbonate ion in water	pK_2	calculate from equation 15	(-)
Fluid dynamic viscosity	η_f	calculate from equation 7	(Pa.s)
Fluid electrical permittivity	ε_f	calculate from equation 5	(F/M)
Fluid relative electrical permittivity	ε_r	calculate from equation 6	(-)
Fluid conductivity	σ_f	calculate from equation 18	(S/m)
Mineral/solution interface			
Surface site density	Γ_s	8.33×10^{18}	(site/m^2)
Disassociation constant For dehydrogenization of silanol	$pK\_$	6.9	(-)
Binding constant for cation adsorption of quartz	pK_{Me}	7.4	(-)
Surface ionic mobility	β_s	5×10^{-9}	(m^2/sV)
Proton conduction	Σ_s^{prot}	3.56×10^{-8}	(S)
Stern plane distance	χ_ζ	2.4×10^{-10}	(m)
Debye length	χ_d	calculate from equation 10	(m)
Stern plane potential	φ_d	calculate from equation 22	(V)
Fundamental physical constants			
Boltzmann's constant	k_b	1.381×10^{-23}	(J/K)
Dielectric permittivity in vacuo	ε_o	8.854×10^{-12}	(F/m)
Avogadro's number	N	6.022×10^{23}	(F/m)
Charge of an electrode	e	1.602×10^{-19}	(mol^{-1})
Atomic mass of CO_2	A	44.01	(g/mol)

* This quantity was calculated by Archie law (Appendix B).

** This quantity was obtained experimentally during the data acquisition part of this research.

3 Experimental model and procedure

In order to verify, whether the modified theoretical model reflects the behavior of zeta potential and streaming potential coefficient (generated by the interaction of CO_2-enriched water and rock mineralogy composition), a series of core flooding experiments was conducted. The experiments were performed using a sequence of increasing and decreasing flow rates for different pore fluid concentrations, at a constant temperature of 30 °C. The experimental conditions and procedures the theoretical approach discussed previously.

To ensure the functionality of the experimental apparatus, and that the initial theoretical model of Glover et al [14] describes the behavior of streaming potential coefficient (C_S), and the ζ potential for the properties of this particular sandstone sample, a base case scenario was created. As a reference experiments were performed with different NaCl solutions in a secondary Fontainebleau sandstone sample, identical to the sandstone sample used for this study (Table 1). The experimental results of this base case are shown in Figure 4. This base case scenario, calibrates our experimental apparatus and establishes the repeatability of the experiments carried out by Glover et al. [14]. An overview of the experimental procedure is in Appendix D.

3.1 Experimental apparatus

A schematic representation of the apparatus used for the core flooding experiments is shown in Figure 5. It includes an injection unit, a pressure control unit, a test unit and two data acquisition systems. The entire apparatus and the data acquisition systems were placed in an isothermal cover with a heat generation system connected to the thermal sensors to ensure temperature stability in the system.

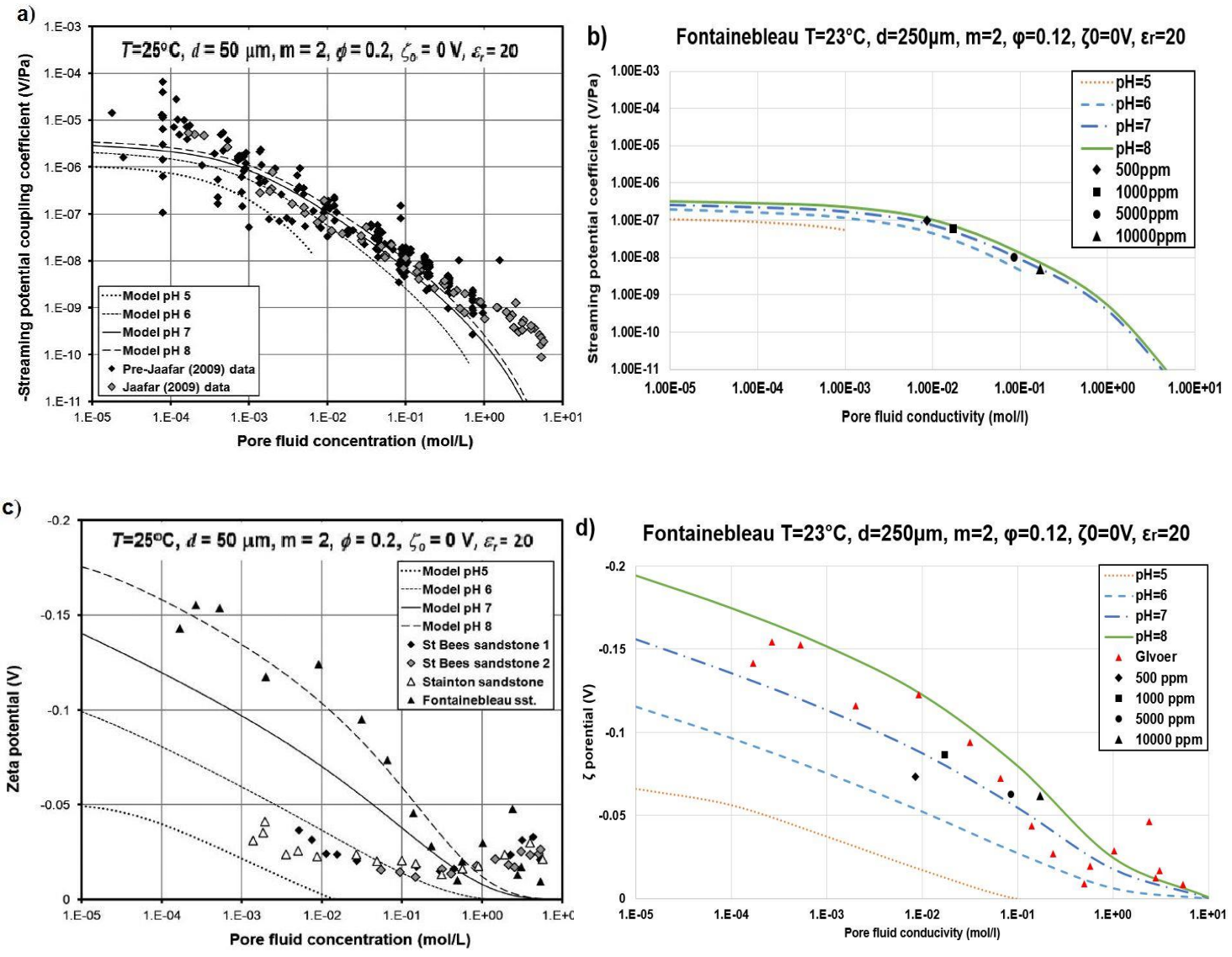

Figure 4. Theoretical estimations and experimental results of NaCl for Fontainebleau sandstone in comparison with data available in the theory. (a) Streaming potential coefficient model obtained from Glover et al. [14]. (b) Streaming potential coefficient model developed for the rock properties of Fontainebleau (Table 1) and experimental results for NaCl solution. (c) ζ potential model obtained from Glover et al. [14]. (d) ζ potential model developed for the properties of Fontainebleau (Table 1) and experimental results for NaCl solutions.

The injection unit consists of a silicone oil tank, a GE P-900 pump and a piston fluid tank. The test unit consist of the core holder device and the pressure control unit which includes a back pressure tank. The first data acquisition system is used only for temperature, pressure and pressure differences measurements, while the second is used for electrical charge and conductivity measurements.

3.1.1 Test unit and sandstone sample

The test sample unit, consists of a cylindrical core holder device (Figure 6) and has been designed such that it tolerates pressure and temperature up to 65 bar and 100 °C respectively. Its total fluid capacity has been calculated to be 142 ml.

The cylindrical shape sample of Fontainebleau SST (Figure 7), contains 99% quartz, its permeability is 16.09 ± 1.43 mD, and it has a porosity of 12% (parameters that coincide with the literature). The average grain diameter is 250 μm and the formation factor is between 145 and 200. It was coated with a layer of glue to ensure that the flow goes through the entire length of the core and no leakage occurs during the experiments. The dimensions of the consolidated sandstone cylinder were 39.5 mm diameter and 170 mm length. The glue increased the width of the sample to 40.5 mm. When the sample was inserted into the cylindrical device, the fit was such that the tolerance was ±0.01 mm. The glue ensures that there is no contact between the sample and the wall, so that there is no influence from external sources. More specific, the influence from external sources can be considered to be the low frequencies generated by the components of the apparatus that are connected to electrical power as well as the low frequency generated by neighboring equipment of the lab. These frequencies are in the magnitude of the scale used in the voltage deference measurements and have a major impact on the noise level.

The holes/sockets for the silver (Ag) electrode transmitters were drilled, with 8 mm diamond drilling bits, after the sample was mounted into the core holder device. Therefore, the assembly was dismounted, cleaned and mounted again, to secure that no failures were made during the drilling procedure. The exact distance between the two sockets was measured (m).

During the experiments, the flow direction through the core was from the bottom to the top and the space between the core and the core holder was completely saturated by the confining pressure fluid.

3.1.2 Data acquisition system and error.

The two devices of interest, from the data acquisition system, are the pressure difference (*ΔP*) transducer and the unit for the voltage potential measurements. These two components contribute considerably to the measurement error of the signal.

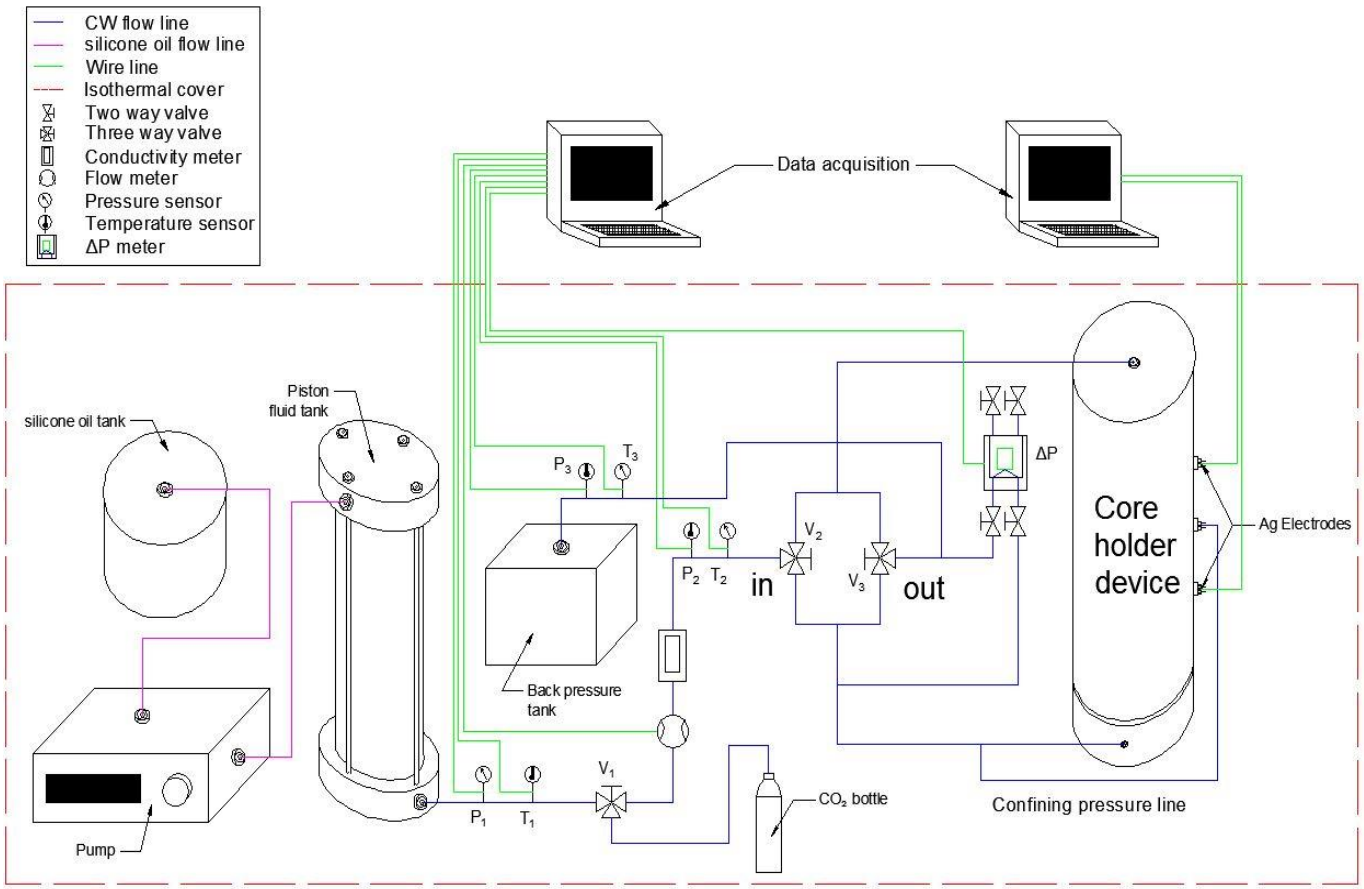

Figure 5. Schematic representation of experimental set-up used for the study of CW behavior on electrokinetic effects.

Precisely, the ΔP meter (Figure 1) used in this apparatus was a Deltabar S from EH (Endress & Hauser) with a full scale output error of 0.3×10^{-6}. The device used for the voltage potential measurements was a digital oscilloscope Yokogawa DL9240L with 8 bit resolution and total output error less than 0.4%. However, because of the influence by the external sources discussed previously, the noise level of the voltage measurements was larger than expected, which significantly affects the total interpretation and thus quantitatively a total error of 5% is estimated. Similarly the pressure data acquired by the ΔP transducer have been corrected according to the temperature variation and the response from the pressure sensors, with a total error of 1% has been estimated on the final interpretation.

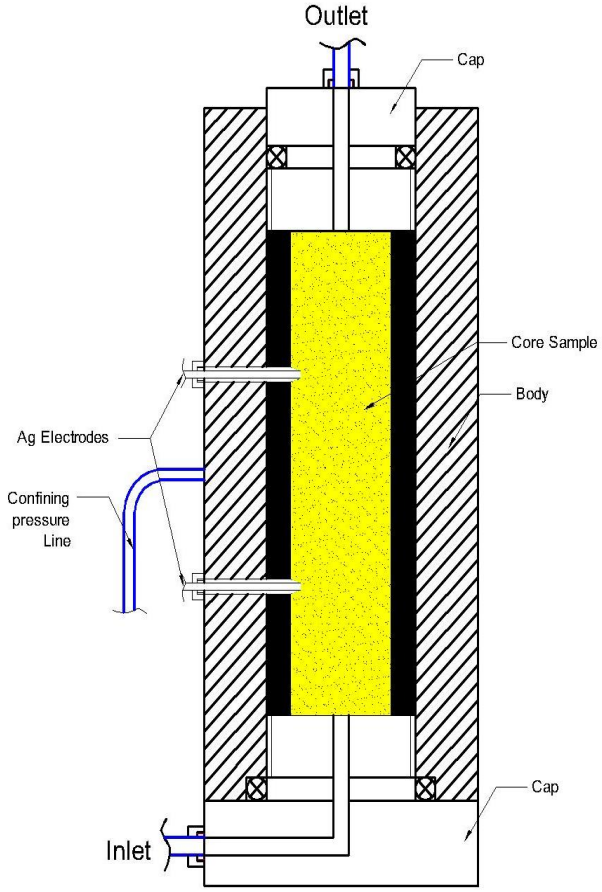

Figure 6. Sketch of cylindrical core holder device.

3.1.3 Injection unit and fluid preparation

The injection unit, consist of a GE P-900 pump, the silicone oil tank and the piston fluid tank. These three components in combination with the CO_2 bottle have a major role during the fluid preparation.

Three equilibrium fluids of CW were prepared and injected for each sample sandstone individually. The preparation procedure is as follows:

- complete demineralized and degassed water was placed into the piston fluid vessel (Figure 8).
- silicone oil was pumped from by the GE P-900 pump till the air was removed completely, without creating any additional pressure.
- simultaneously, the demineralized degassed water was heated at 30 °C.
- the CO_2 bottle of 1 liter capacity was filled and pressurized under the favorable pressure of the equilibrium, in this case 7, 12 and 18 bar.
- thereafter, the CO_2 bottle was connected to the three way valve V_1 (Figure 5), where the CO_2 was injected in small quantities and mixed with the demineralized water until pressure stability between the CO_2 bottle and the vessel was achieved (equilibrium point).

This procedure was repeated for all the equilibrium fluids. The volumes of demineralized water and CO_2 were measured for concentration calculation. Note that in the equilibrium phase during the pressure steps, the system pressure was always above the point where CO_2 could degassing.

Figure 7. Core sample of Fontainebleau sandstone drilled and covered with glue.

3.2 Experimental procedure and data acquisition

The experiments were conducted in a procedure consisting of two stagers; the system preparation and the experimental test. The overall process, for the acquisition of the data presented in paper, was repeated for the three equilibrium fluids, mentioned in Table 2.

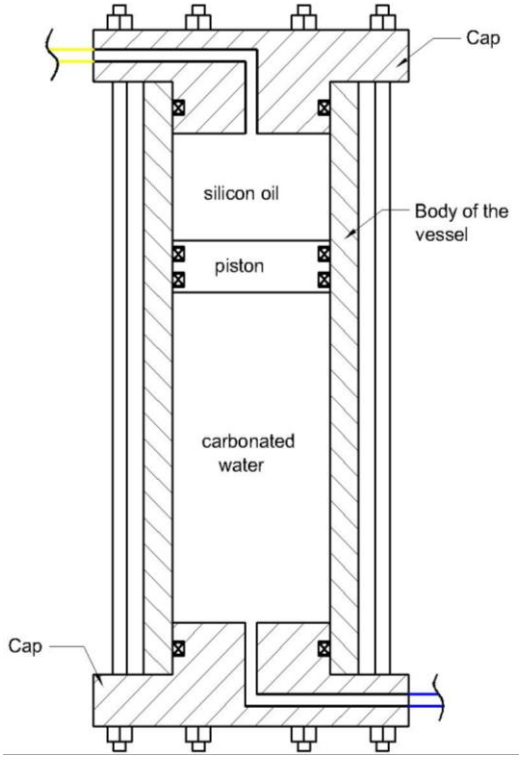

Figure 8. Piston fluid vessel representation, major component in both the preparation and the fluid injection.

3.2.1 System preparation

There are three steps in the system preparation part of the experimental procedure; the mounting of the core, the replacing of fluids and, most importantly, the system regulation.

When the core sample was placed in the system, the following procedure was followed. The experimental apparatus was dried with continuous injection of CO_2 at 5 bars, with the injected amount of CO_2 of at least 10 pore volumes. The CO_2 was preplaced by injection of demineralized and degassed water at 19 bar stable system pressure. The amount of demineralized degassed water injected, always exceeded 4 pore volumes and the injection was taking place, at a relative high pressure to dissolve any remaining CO_2 that was trapped or accumulated in the pore space of the sample. Thus, no CO_2 gas was present in the system.

Once the apparatus was filled with DM & DG water, the pressure of the system was regulated, from the back pressure tank, and stabilized at the same pressure with the wanted equilibrium fluid (Table 2), which was connected to the system. In this stage the apparatus was prepared for the data acquisition or experimental testing part.

When the data acquisition part was finished and the next equilibrium fluid was prepared in the injection unit, the system was flushed again with DM & DG water at 19 bar system pressure for the same reasons discussed previously. In this step, the total volume injected was exceeding 4 pore volumes to ensure that no CO_2 resides in the volume of the system.

All the steps mentioned above were always completed under constant temperature of 30 °C. All the injections were performed with a Teledyne 1000D ISCO Pump, which was connected with the system by the valve V_1 (Figure 5). After the equilibrium fluid was prepared, the CO_2 bottle was replaced by the ISCO pump for the water injection.

3.2.2 Experimental test / data acquisition

The data acquisition include four distinct measurements, which are permeability measurements, CW streaming potential measurements and pore fluid electrical conductivity measurements. The permeability measurements, were conducted before any CW solution was injected into the system and the results are given in Table 1.

The injection of CW fluid was completed and regulated by the injection unit. Before any measurement was conducted, at least 3 pore volumes were injected through the system to achieve full saturation of the core sample and to secure the integrity of the measured data.

The measurements of pressure and voltage is strongly correlated with flow rates. The overall acquisition was performed by measuring the response for different flow rate values regulated from the injection unit. The overall process can be described as:

- CW was injected from the vessel through the system in a stable low flow rate of 0.5 ml/min, which was established as a minimum reference point.
- The flow rate was regulated by the GE P-900 pump and it was increased a maximum value and decreased back to the reference point, stepwise, by 0.2, 0.5 or 1 ml/min (was chosen according to the range limit of the ΔP meter). The temperature, pressure difference, and voltage difference values were recorded for each step but only after the responses were stable.
- The pore fluid electrical conductivity was recorded throughout the same acquisition procedure.

These steps were repeated for all the equilibrium fluids on the Fontainebleau sample. After each measurement was completed, DM & DG water was injected at relative high pressures to remove the electrolyte solution and the apparatus was prepared for the injection of the next electrolyte solution, according the technique explained previously. The range of the flow rates applied for each ionic fluid during the acquisition, as well as the range of data recorded, are displayed in Table 2. The temperature variation obtained during the experiments were used for the correction of the values compared to the initial conditions.

3.3 Quantities calculation

One of the major goals of this study, is to investigate whether this theoretical model can describe the zeta potential (ζ) behavior and streaming potential coefficient (C_s) as a function of pore fluid concentration (C_f), within a range of acidic *pH* environments. However, the experimental apparatus was not developed to provide measured values of pore fluid concentration and *pH*. Consequently, those two quantities were calculated by the methods explained hereafter.

Table 2. Ranges of the values that were used or recorded during the experimental part of this research topic. The values of pressure difference, voltage difference and the calculated streaming potential coefficient have been corrected according to the reciprocal recorded temperature.

Equilibrium fluid pressure (bar)	Q (ml/min)	ΔP (MPa)	ΔV (V)	CS (V/Pa)
		Fontainebleau SST		
7	0.5 – 2	0.249 – 1.689	0.121 – 0.272	5×10^{-7}
12	0.5 – 3	0.765 - 2.859	0.189 – 0.230	6×10^{-7}
18	0.5 – 2.5	0.359 – 1.642	0.065 – 0.117	3×10^{-7}

3.3.1 Pore fluid concentration (C_f) of equilibrium fluids

The literature gives three methods, compatible for this study that can be used for the estimation of the CW concentration. These can be classified as volumetric and non-volumetric. The non-volumetric method is to measure conductivity values for the estimation of molar concentration while the volumetric methods comprise those that use the ideal gas law and the modified Henry's law. For this research we are interested in the volumetric methods, mainly because we are dealing with measured quantities with higher precision.

The concentration calculation of the ionic equilibrium fluids was computed by both volumetric methods using the Boyle & Gay-Lussac and the modified Henry's law, defined as:

$$PV = nRT \tag{25}$$

The Boyle & Gay-Lussac equation for ideal gases; P (Pa) is current the pressure; V (l) refers to the total volume; n (mol) is the number of moles; T (K) is the temperature; and R = 8.3145 (J/molK) is the ideal gas constant.

$$c_{tot} = p/H' \tag{26}$$

The modified Henry's law is used to described the equilibrium relation between vapor and liquid where, c_{tot} represents the equilibrium mole fraction in the liquid face; p (Pa) stands as the partial pressure; and H' (Pa) is the Henry's constant. A more detailed description of Henry's law in equilibrium fluids can be found in Appendix E.

The results of the CO_2 concentration calculations for the equilibrium CW ionic fluids in Table 3, together with their corresponding errors.

Based on the error analysis conducted for the two volumetric methods it has been observed that Henry's law produces more accurate values than the Ideal gas law. In addition, with the previous observation, the fact that CW is not an ideal solution makes the estimations from the ideal gas law inaccurate. Therefore, the results obtained by Henry's law as more consistent for the interpretation of our experimental results.

Table 3. Summary of pore fluid concentration calculated with volumetric methods included error.

Pore fluid concentration (mol/l)		
Equilibrium fluids (bar)	**Ideal Gas**	**Henry's law**
	Fontainebleau SST	
7	$0.044 \pm 7 \times 10^{-3}$	$0.029 \pm 3 \times 10^{-3}$
12	$0.06 \pm 3 \times 10^{-2}$	$0.079 \pm 6 \times 10^{-3}$
18	$0.134 \pm 8 \times 10^{-3}$	$0.178 \pm 1 \times 10^{-2}$

3.3.2 Pore fluid *pH* on equilibrium CW

In carbonic chemistry one method for the estimation of *pH* for CO_2-H_2O systems is based on the Bjerrum plot, which is widely used in the field of oceanography. It represents the equilibrium between the carbonate species of $[CO_2]$, $[HCO_3^-]$ and $[CO_3^{2-}]$ as a function of pore fluid concentration (C_f) [56]. We consider this method as suitable, because it is sensitive to salinity and to temperature variation [54]; two factors that also exist as variables in the theoretical model. This method can be applied within the temperature ranges we use.

The two equilibrium chemical reactions that occur during the dissolution of CO_2 in water are explained in equation 12 and 13. The equilibrium concentrations of carbonate ions individually can be calculated by a set of three equations which are given as [55]:

$$[CO_2] = \frac{[H^+]^2}{[H^+]^2 + K_1[H^+] + K_1K_2} \times c_{tot} \quad (27)$$

$$[HCO_3^-] = \frac{K_1[H^+]}{[H^+]^2 + K_1[H^+] + K_1K_2} \times c_{tot} \quad (28)$$

$$[CO_3^{2-}] = \frac{K_1K_2}{[H^+]^2 + K_1[H^+] + K_1K_2} \times c_{tot} \quad (29)$$

where, K_1 and K_2 are the two equilibrium dissociation mentioned before; c_{tot} is the total concentration of the species. More details for the equations above are included in Appendix F.

The *pH* values for the ionic fluids with their corresponding error as well as Bjerrum plot suitable for the experimental conditions (30 °C and zero salinity) are displayed in Table 4 and Figure 9 respectively.

Table 4. List of the estimated pH values obtained by the concentrations of the CW ionic fluids.

pH values for CW fluids used in experiments	
Equilibrium fluids (bar)	**Corresponding pH**
Fontainebleau SST	
7	$4.76 \pm 3.81 \times 10^{-2}$
12	$5.05 \pm 6.06 \times 10^{-2}$
18	$5.3 \pm 1.07 \times 10^{-1}$

3.3.3 Prediction of ζ potential values

As it is reported by Glover et al. [14], Pride and Morgan [8] (1991) created a relation to interpret the experimental data of NaCl solution with zeta potential. This empirical relationship links the pore fluid concentration with ζ potential such as:

$$\zeta(mV) = a + b\log(C_f) \quad (30)$$

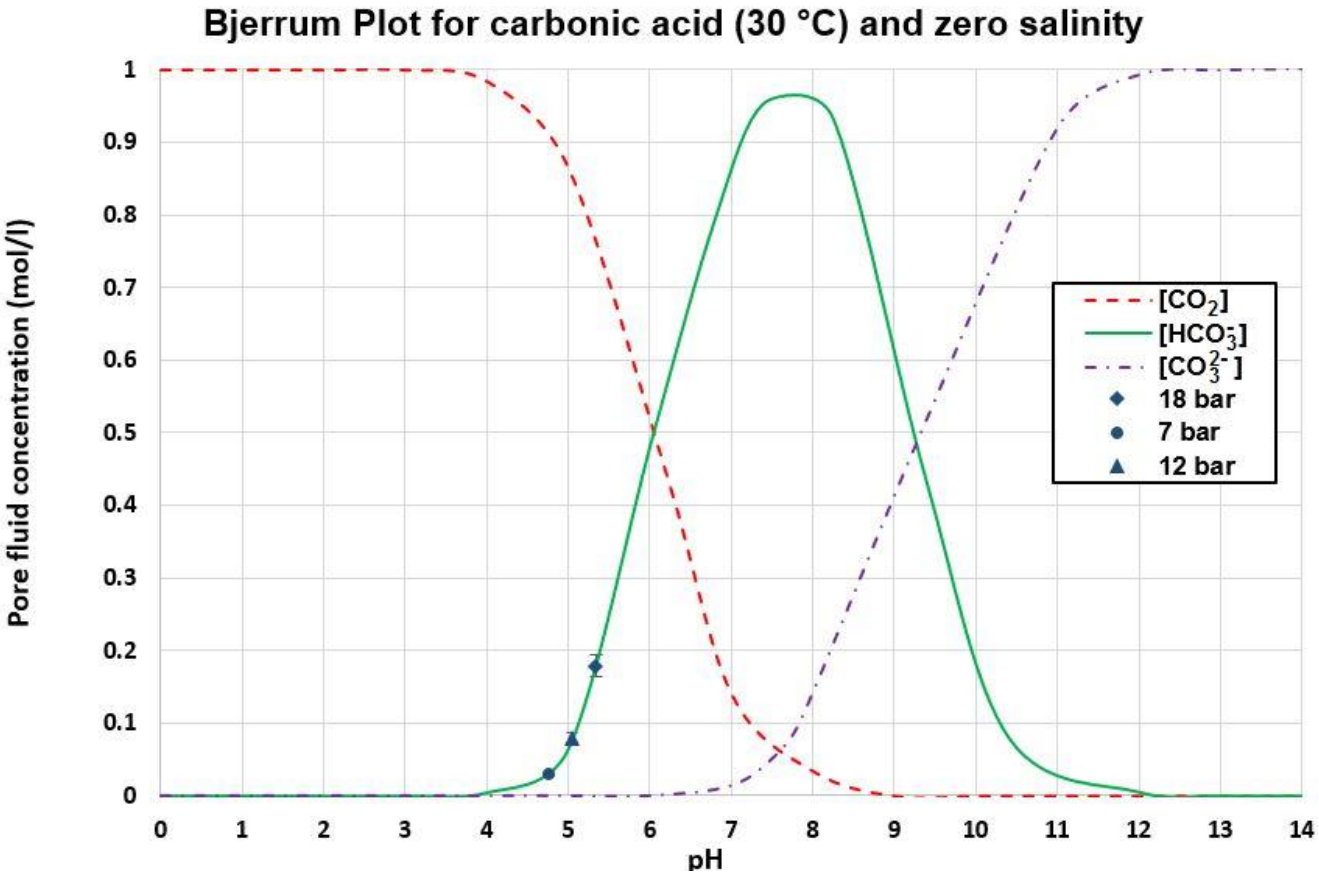

Figure 9. Bjerrum plot of the equilibrium CW solutions used for the flooding experiments in Fontainebleau sandstone

Revil et al. [4] and Jaafar et al. [57] studied this relation over a wide range of data and they suggest that the two parameters *α* and *b* are -6.43 and 20.85 respectively [14].

Despite the fact that this function was established for low and medium salinity fluids, it was used in this research to predict *ζ* potential from CO_2-enriched water under the assumption that it can generate accurate values for any electrolyte solution. The results of *ζ* potential for the CW concentrations are listed in Table 5.

Table 5. List of ζ potential values.

ζ potential estimations	
Pore fluid concentration (mol/l)	**ζ (V)**
$0.029 \pm 2 \times 10^{-3}$	-0.038 ± -0.0031
$0.079 \pm 6 \times 10^{-3}$	-0.030 ± -0.0024
$0.178 \pm 1.4 \times 10^{-2}$	-0.022 ± -0.0018

4 C_S Coefficient and curve fitting results

The interpretation of the recorded data and the theoretical results can be separated into the quantification of the streaming potential coefficient and the interpolation of the theoretical model with the experimental data.

4.1 Experimental results and coefficient

The data acquisition was performed with both increasing and decreasing sequence of flow rates, under a stable system pressure equal to that of equilibrium fluids and at a temperature of 30 °C. Figures 10a and 10b show a schematic representation of the stabilized voltage and the stabilized pressure difference (ΔP) against time for a single flow rate. In Figure 10a it can be observed that due to the noise level, generated by external sources (frequencies from the apparatus components and neighboring lab equipment), the voltage difference (ΔV) needs filtering. The voltage difference (ΔV) for each flow rate was estimated based on the average values of the stable regimes. A similar phenomenon was observed in the stabilized pressure difference data, for which a schematic representation is given in Figure 10b, and similarly an average stabilized pressure difference was

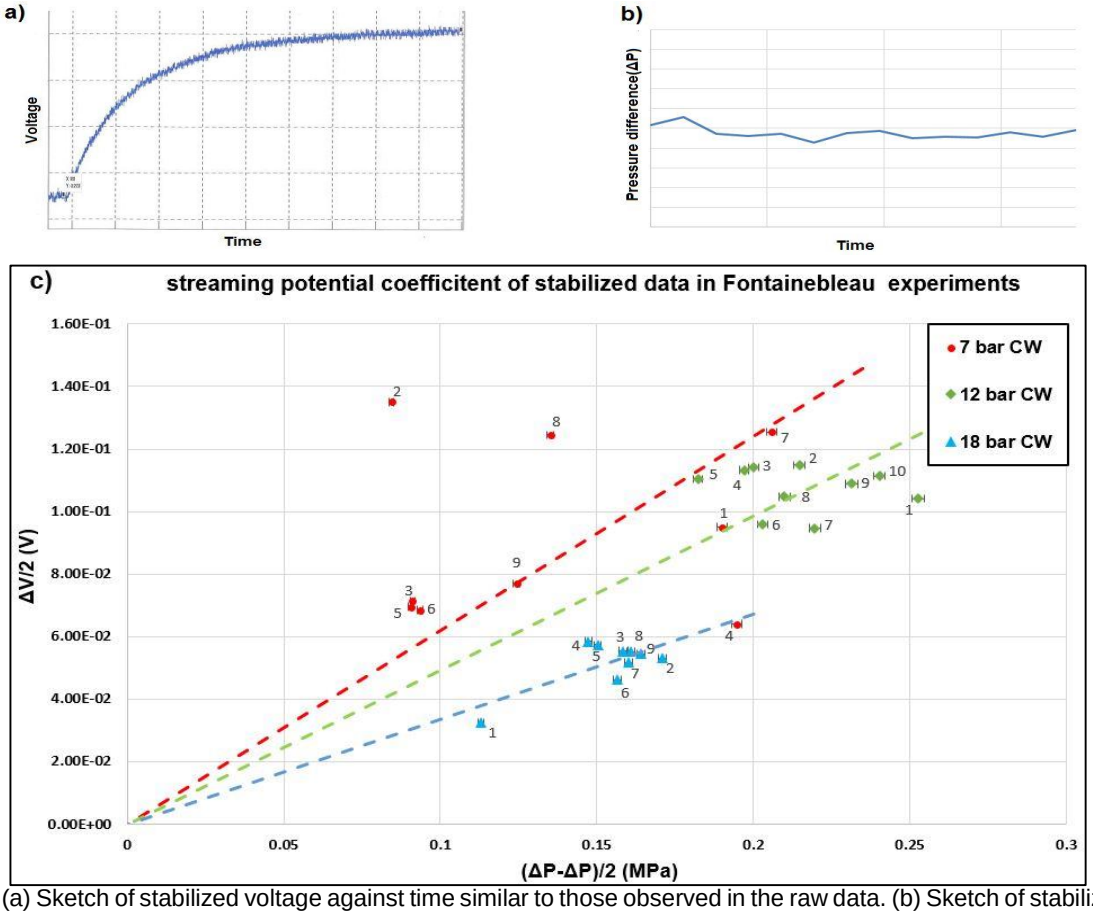

Figure 10. (a) Sketch of stabilized voltage against time similar to those observed in the raw data. (b) Sketch of stabilized pressure difference (ΔP) against time similar to those observed in the raw data. (c) Stabilized voltage differences (ΔV/2) and pressure differences ((ΔP_{prev}- ΔP)/2) 8experimental data with the corresponding coefficient lines.

obtained for each flow rate. Following the interpretation method of Vinogradov et al. [58], the stabilized data for both increasing and decreasing flow rates are plotted together in Figure 10c, where each point represents a pair of a stabilized average pressure differences ((ΔP_{prev}- ΔP)/2) and stabilized average voltage difference ($\Delta V/2$) for a single flow rate. The static potential has been eliminated. The numbers of the data refer to the sequence of the steps through time. Specifically, for all the ionic fluids the point values with numbers between 1 and 5 represent increasing flow rate while the number above 5 denote decreasing flow rate. Vinogradov et al. [58] states that the advantage of this method is that the measured data can be interpreted without monitoring the static potential.

Figure 10c, shows that ΔV is increasing with increasing ΔP, but the deviation of the scatter is more pronounced from the expected linear behavior, especially in the data of the 7 bar equilibrium fluid. In this work, we are interested in the interpretation of this spread with the coefficient line. It results in a single value for the streaming potential coefficient (C_S). The degree of the coefficient individually for the data points of each equilibrium fluid are presented in Figure 10c.

4.2 Physical relation and zeta offset (ζ_0)

Glover et al. [14] in 2012 developed a model to predict zeta potential and streaming potential values over a range of fluid concentration for different *pH* environment. They implemented their theoretical model to a wide range of experimental data, obtained from literature. To achieve an accurate interpolation, they modified equation 23 by introducing a new coefficient named zeta offset (ζ_0), which varies between 0 and -0.035 (V). This coefficient can be characterized as a correction factor in the Debye-Huckel approximation formula, which in their publication was replace by [14]:

$$\zeta = \varphi_d \ \exp(-\chi_\zeta/\chi_d) + \zeta_0 \qquad (31)$$

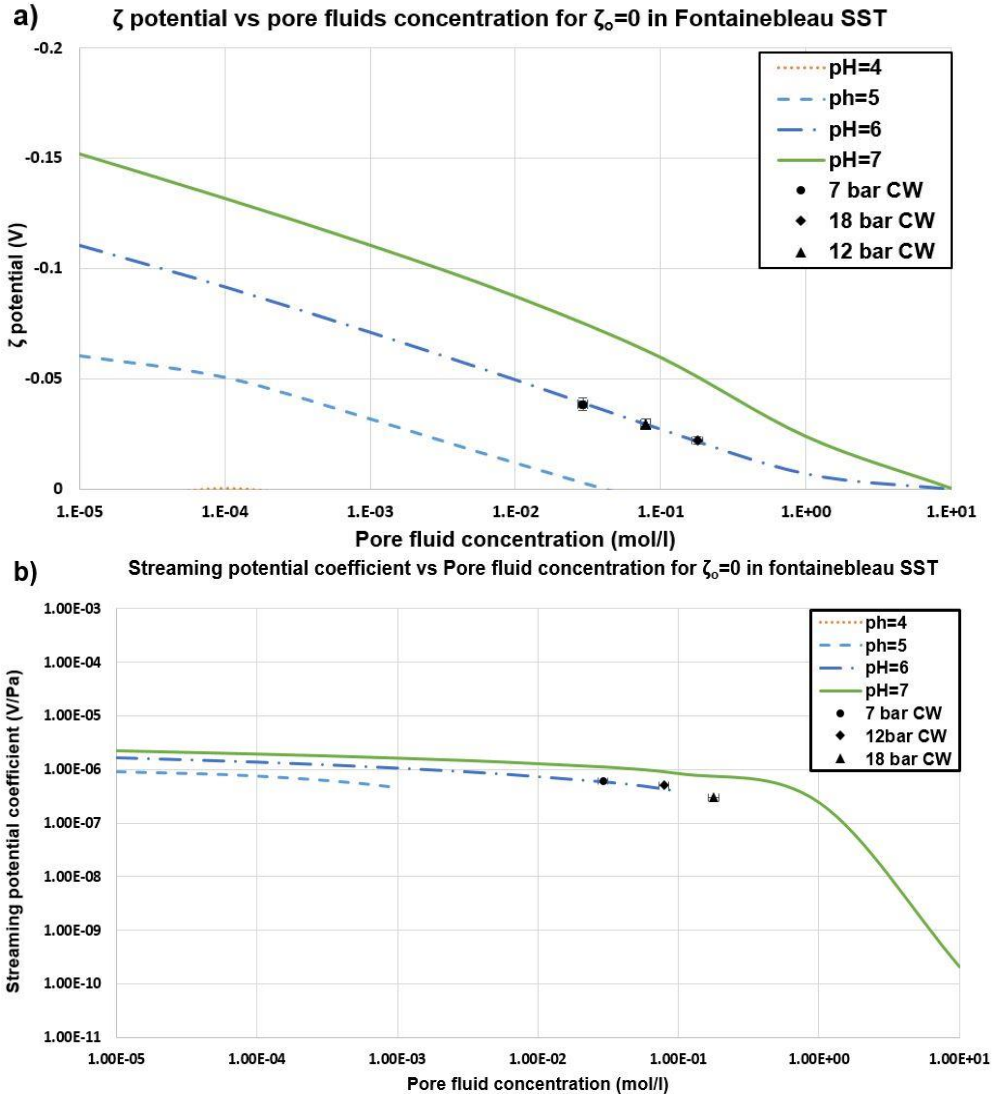

Figure 11. Combination of streaming potential coefficient (C_S) and zeta (ζ) potential models as a function of pore fluid concentration implemented for the experimental values for zero zeta offset ($\zeta_0=0$). (a) Zeta (ζ) potential model for CW flooding in Fontainebleau SST sample. (b) Model of streaming potential coefficient (C_S) for CW flooding in Fontainebleau SST sample.

In their fitting procedure they modified several rock and fluid parameters such as porosity (φ), formation factor (F), electrical relative permittivity (ε_r) and grain size (d).

In the interpolation procedure of this research topic the fluid and the rock parameters are maintained as constants. Equation 31 was applied here to fit the theoretical model to the experimental data by the variation of ζ_0. To keep this theoretical model in line with the approach of Glover et al. [14], the variation range of the zeta offset was kept within the same range of 0 and -0.035 (V). Three cases were selected and are presented, developed with different zeta offset values. The purpose of those models is to investigate the behavior of ζ potential and streaming potential coefficient within an acidic environment and thus the *pH* range of interest is within 4 to 7.

A combination of both models for the first case (zero zeta offset) are in Figure 11. In the model of the ζ potential (Figure 11a) it is visible that the theoretical estimations are lower than experimental data, and are intercepting with a line of higher *pH* estimations than those calculated by Henry's law previously. Similar phenomenon is observed in the streaming potential coefficient model (Figure 11b). In addition, it can be noted that the theoretical values of *pH* 4 in two models are hardly visible or non-existing, due to the fact that the estimated ζ values for low *pH* become positive at relative low CW concentration values.

The models for the second case, reflect the implementation of the theoretical estimations to the experimental measurements with a zeta offset value of -0.020 (V) (Figure 12). Here, it shows that there is an improvement in comparison with the previous case. However, the *pH* remains at a higher range with respect to the calculated values for the CW solutions used in the experiments. Furthermore, in the C_S model of the sandstone sample (Figures 12b) a more linear behavior of streaming potential

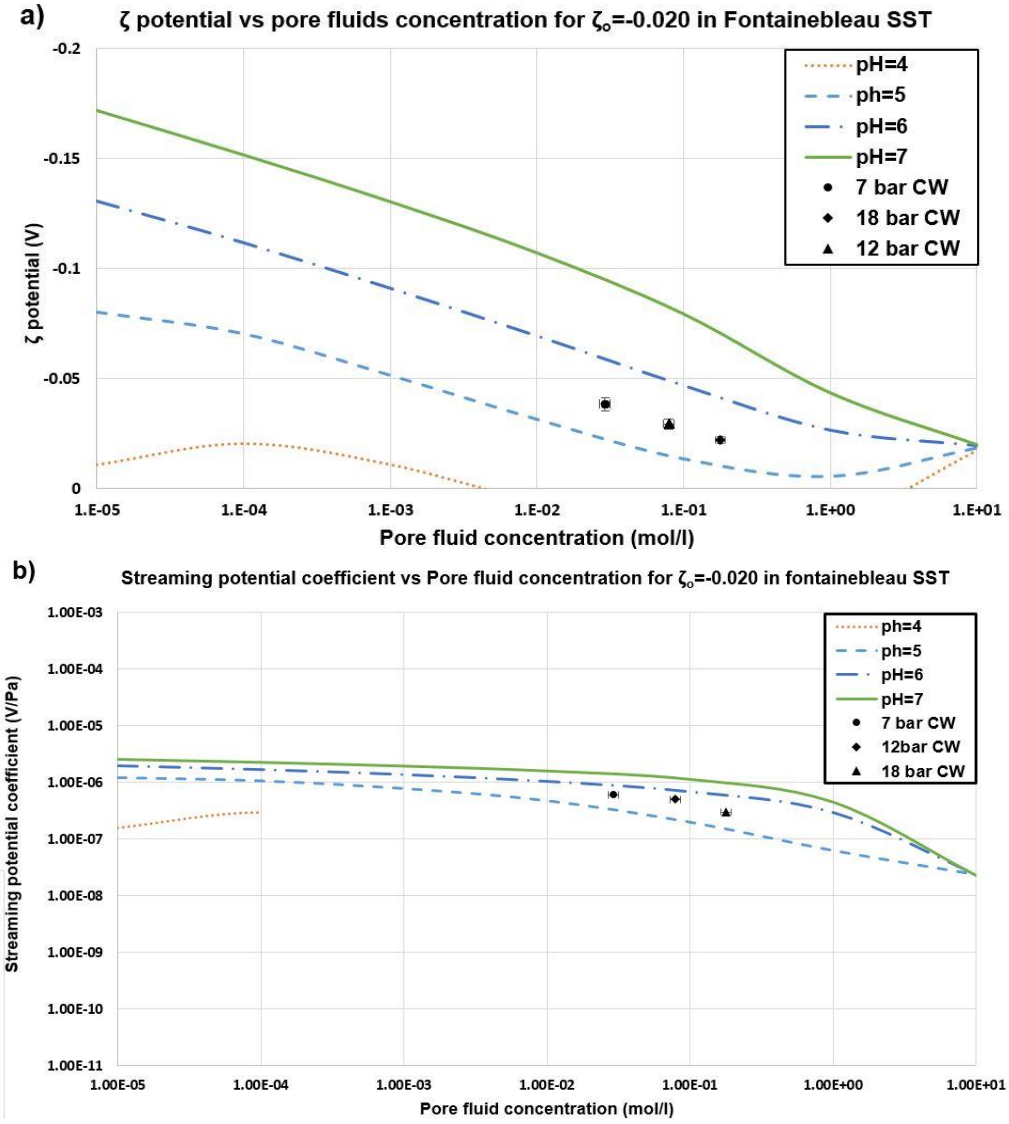

Figure 12. Couples of streaming potential coefficient (C_S) and zeta (ζ) potential models as a function of pore fluid concentration implemented for the experimental values for -0.020 (V) zeta offset. (a) Zeta (ζ) potential model for CW flooding in Fontainebleau SST sample. (b) Model of streaming potential coefficient (C_S) for CW flooding in Fontainebleau SST sample.

and a smaller decrease at relative higher concentrations is observed in contrast to the first case.

The best match of the interpolation was obtained in the third case where the zeta offset was defined as -0.034 (V) (Figure 13). The experimental results of CW flooding in Fontainebleau sample are matching successfully with the theoretical estimations on the line of *pH* of 5; a value close to those calculated for the different concentrations of the equilibrium CW solutions (Table 4). In Figure 13a, it is visible that the model of *ζ* potential for the Fontainebleau sandstone are extrapolating very well with the experimental value of 12 bar, while the corresponding values for 7 bar and 18 bar are in higher and lower ranges respectively. A similar phenomenon is visible in Figures 13b, where the streaming potential coefficient (C_S) extrapolates in line with the point value of 12 bar, while a small difference between the experimental point values (of 7 and 18 bar) and the assumed estimations has been observed. It is still debatable whether this deficiency is a contribution of the coefficient in combination with the parameters *α* and *b* of equation 30, used in the approximation of *ζ* potential, or is attributed to the sensitivity in the parameters of the theoretical model.

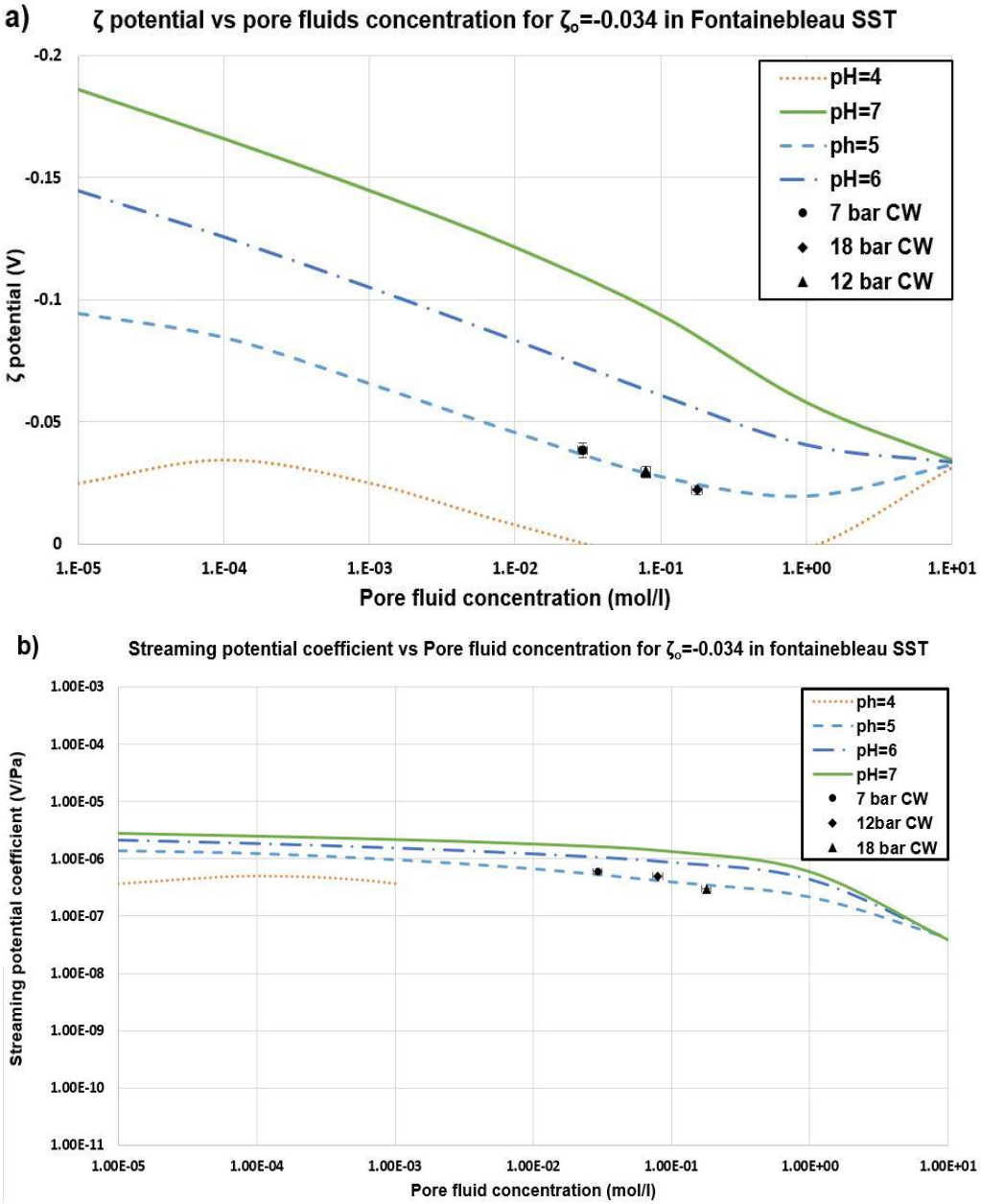

Figure 13. Couples of streaming potential coefficient (C_S) and zeta (ζ) potential models as a function of pore fluid concentration implemented for the experimental values for -0.035 (V) zeta offset. (a) Zeta (ζ) potential model for CW flooding in Fontainebleau SST sample. (b) Model of streaming potential coefficient (C_S) for CW flooding in Fontainebleau SST sample.

5 Conclusions and Discussion

In this work we investigate the hypothesis of whether existing models of zeta potential (ζ) and streaming potential coefficient (C_S) for NaCl solutions can provide accurate estimations under modifications for CW flooding in reservoir rocks with small amount of clay. For this investigation the model of Glover et al [14] was selected and converted successfully to a new modified model, which accounts for CW. To validate the theoretical results, experiments in a sample of Fontainebleau SST were performed with different concentrations of CW.

The scatter of the experimental results is relatively larger than the expected theoretical linear behavior between voltage difference (ΔV) and pressure difference (ΔP). The most plausible explanation for this phenomenon is the influence from the noise generated by the low frequencies originating from the neighboring equipment of the lab and the components of the experimental apparatus connected to electrical power. For the correlation of these values with the theoretical model a streaming potential coefficient (C_s) was obtained individually for each equilibrium fluid. For similar CW flooding experiments in sandstone samples with similar rock properties and higher clay content, lower streaming potential values are expected. This phenomenon has been also detected and reported in the corresponding literature for low salinity fluids.

The suggested theoretical model generated logical values of the ζ potential and the streaming potential coefficient (C_S) for CW flooding within a *pH* range of 4 to 7 (acidic environment) for different CO_2 fluid concentrations. The model remains sensitive to temperature, salinity, reservoir rock properties and fluid properties; the main variable is the fluid concentration (C_f). Following the approach of Glover et al. [14], the parameter of zeta offset (ζ_0) was implemented as a correction factor on the theoretical estimations. From the comparison of the theoretical estimations with the experimental results, it can be concluded that this model describes the behavior of streaming potential coefficient and zeta potential for CW flooding in low clay content rocks. Additionally, it was observed that the theoretical model reproduces the shape of the experimental results for the Fontainebleau sandstone sample. It can be concluded that this model can be used for estimations of ζ potential and streaming potential coefficient (C_S) in different CW concentrations.

At the current stage studies concerning the dielectric aspects of ionic fluids aside from low salinity fluids are limited. Especially, the area of CO_2 dielectric behavior in reservoir rocks is currently in a premature stage. Further studies would improve the current knowledge significantly.

The theoretical model discussed in this study can be characterized as successful. However, the physics behind the need for the parameter of zero offset (ζ_0) is still a matter of debate. According to Glover et al. [14], a possible cause may be the theoretical approximation of electrical permittivity. A sensitivity study on the approximation of the parameters should be conducted.

For further experimental work it is strongly recommended that the time interval between the measurements should be large (e.g. 20 minutes). It may result in a more linear behavior of the spread between the pressure difference and the voltage difference. In addition, it is recommended that *pH* of the fluid should be measured individually for each measurement during the experiment and not calculated theoretically, which may decrease the uncertainty of the measurements during the correlation with the theoretical model.

Finally, it is suggested that further modification and application of this model be performed in a wide range of ionic fluids used for EOR methods and reservoir rocks with relatively higher clay content.

6 Acknowledgements

This research would never be possible without the support of CATO2 project (CO_2 capture, transport and storage in the Netherlands). Particularly, I would like to express my gratitude to Dr. Karl-Heinz A. A. Wolf, for his guidance, devotion and most importantly inspiration he has provided me during this project. Special thanks to Prof. Dr. Pacelli L.J. Zitha for his guidance, encourage and his overall contribution.

Appreciation should be granted to Dietz Laboratory of Delft University of Technology where the experiments were conducted and namely to Karel Heller and to Marc Friebel for their help in the laboratory and their overall contribution in this project. I would like also to thank Anna E. Peska who contributed as an external researcher and Faisal Al Saadi who provided the samples of Fontainebleau sandstone.

Finally, thanks to Nikos Tzanavaris, Rahul Prabhakaran, Katerina G. Rigas and Alexios Kotsakis for their scientific and their sociological support.

Appendix A

Electric Double Layer

At any electrode immersed in an electrolyte solution, a specific interfacial region is formed. This region is called the double layer [48]. Electric double layer (EDL) is nothing more than a redistribution of ions in the electrolyte solution to compensate for the surface charge of the rock/clay [49]. This surface charge will attract counter-ions (ions with the opposite charge), which due to entropy will remain dispersed and mobile in the solvent in the vicinity of the surface. On the other hand co-ions (ions with same charge) will be repulsed away from the surface. Essentially, this spatial separation of charge between the two compact layers of charges formed at the electrode/electrolyte interfaces was called the “electric double layer” (EDL). [50, 51].

The concept that a double layer exist at the surface of a solid that is in contact with an electrolyte was introduced by Helmholtz in 1879. That first theoretical model assumed the presence of a compact layer of ions in contact with the

charged metal surface. The next model of Gouy and Chapman involves a diffuse double layer in which the accumulated ions, due to the Boltzmann distribution, extend to some distance from the solid surface. Finally, in 1924 Stern suggested that the electrified solid-liquid interface includes both the rigid Helmholtz layer and the diffuse one of Gouy-Chapman [48]. These three models are shown in Figure A.1. below.

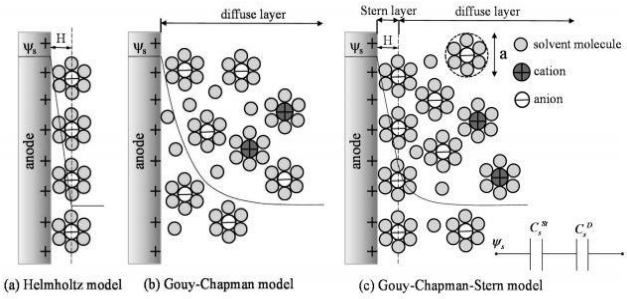

Figure A.1. Sketch of the electrical double layer showing the difference between the models available in the literature, taken from Wang et al. [51]. (a) Helmholtz model. (b) Gouy-Chapman model. (C) Gouy-Chapman-Stern model.

Appendix B

Formation factor (F)

Archie in (1942) defined *F* as the ratio of the resistivity of a saturated formation (R_b) to the resistivity of pore-water (R_w), i.e.

$$F = \frac{R_b}{R_w} = \frac{R_t}{R_o} = I_R, \tag{B-1}$$

For sediments and sedimentary rocks, Archie (1942) developed the following equation, which was later modified by Winsauer et al. (1952), and thus known as the Archie-Winsauer equation, showing the dependence of *F* (dimensionless) on φ (fractional) in relation to α and *m*, where both are dimensionless:

$$F = \frac{a}{\varphi^m} \tag{B-2}$$

which yields,

$$m = -[(logf - loga)/(log\ \varphi)], \tag{B-3}$$

The cementation factor, m, indicates reduction in the number and size of pore openings or reduction in the closed-off (deadend) channels. It is defined as the logarithm of throat area divided by the logarithm of pore area (inverse of the nonlogarithmic definition of aspect ratio; pore area/throat area). This definition of m suggests that the closer the value of throat radius to pore radius, the closer the value of m to unity. For unconsolidated sediments, a value of around 1 is generally used for a [52]. Thus, the Archie-Winsauer equation takes the form:

$$m = -[logf/(log\ \varphi)], \tag{B-4}$$

Appendix C

Cubic equation for pH calculation

As was noted before the solution of equation 17 can be found in appendix of Glover et al. 2012 [15]. This solution follows the Tartaglia-Cardano methodology. A cubic equation can be defined as:

$$x^3 + ax^2 + \beta x + \gamma = 0, \tag{C-1}$$

To link the parameters of equation 17 with the parameters of the equation C-1 let $\alpha = C_a - C_b$, $\beta = -(K_w + K_1)$ and $\gamma = 2K_1K_2$. In addition the quadratic term of equation C-1 can be eliminated by defining:

$$\begin{aligned} x &= y - \frac{a}{3}, \\ A &= \frac{3\beta - \alpha^2}{3}, \\ B &= \frac{2\alpha^3 - 9\alpha\beta + 27\gamma}{27}, \end{aligned} \tag{C-2}$$

Based on the equation C-2, the equation C-1 takes the form:

$$y^3 + Ay^2 + B = 0, \tag{C-3}$$

and the discriminant of the equation above can be written as:

$$D = \frac{A^3}{27} + \frac{B^2}{4}, \tag{C-4}$$

There are three possible solutions of the equation C-1, based on the discriminant value. More specifically, if D > 0, then there are three roots but only one is real, which yield:

$$y_1 = \left(-\frac{B}{2} + \sqrt{D}\right)^{\frac{1}{3}} + \left(-\frac{B}{2} - \sqrt{D}\right)^{\frac{1}{3}}, \tag{C-5}$$

$$\begin{aligned} y_2 = &-\frac{1}{2}\left(\left(-\frac{B}{2}+\sqrt{D}\right)^{\frac{1}{3}} + \left(-\frac{B}{2}-\sqrt{D}\right)^{\frac{1}{3}}\right) \\ &+ \frac{\sqrt{(3)}i}{2}\left(\left(-\frac{B}{2}+\sqrt{D}\right)^{\frac{1}{3}} + \left(-\frac{B}{2}-\sqrt{D}\right)^{\frac{1}{3}}\right), \end{aligned} \tag{C-6}$$

$$\begin{aligned} y_3 = &-\frac{1}{2}\left(\left(-\frac{B}{2}+\sqrt{D}\right)^{\frac{1}{3}} + \left(-\frac{B}{2}-\sqrt{D}\right)^{\frac{1}{3}}\right) \\ &- \frac{\sqrt{(3)}i}{2}\left(\left(-\frac{B}{2}+\sqrt{D}\right)^{\frac{1}{3}} + \left(-\frac{B}{2}-\sqrt{D}\right)^{\frac{1}{3}}\right), \end{aligned} \tag{C-7}$$

where, *i = 1,2* or *3* with respect to the number of the root that we are interested to calculated. If *D = 0*, there are three real roots defined as:

$$y_1 = \left(-\frac{B}{2} + \sqrt{D}\right)^{\frac{1}{3}} + \left(-\frac{B}{2} - \sqrt{D}\right)^{\frac{1}{3}}, \quad \text{(C-8)}$$

$$y_2 = y_3 = -\frac{1}{2}\left(\left(-\frac{B}{2} + \sqrt{D}\right)^{\frac{1}{3}} + \left(-\frac{B}{2} - \sqrt{D}\right)^{\frac{1}{3}}\right), \quad \text{(C-9)}$$

And if *D < 0*, there are three real roots that, which be calculate by:

for *B > 0*

$$y_i = 2\sqrt{-\frac{A}{3}}\cos\left(cos^{-1}\left(-\sqrt{-\frac{27B^2}{4A^3}}\right) + \frac{2\pi k_i}{3}\right), \quad \text{(C-10)}$$

for *B > 0*

$$y_i = 2\sqrt{-\frac{A}{3}}\cos\left(cos^{-1}\left(\sqrt{-\frac{27B^2}{4A^3}}\right) + \frac{2\pi k_i}{3}\right), \quad \text{(C-11)}$$

Appendix D

Base case scenario with NaCl solution

The additional experiments NaCl were conducted on a external Fontainebleau sandstone sample, to ensure that the experimental apparatus is functional and the initial theoretical model without fluid modifications can describe the behavior of zeta potential for the sandstone sample of Fontainebleau. The overall procedure that was followed during the experiments was in line with the procedure used for CW.

More specifically, after the core sample was mounted to the core holder, the system was dried with continuous injection of CO_2 at 5 bar (5 pore volumes were produced). Further, the CO_2 was completely removed from the system with injection of demineralized and degassed water at 8 bar (4 pore volumes were produced). The system pressure was defined at 7 bar. Thought all the system preparation the temperature preserved constant at 23°C.

Four experiments were conducted with different NaCl concentration. The measurements were acquired by the modification of flow rate under constant system pressure and temperature of 7 bar and 23°C respectively. The injection of the NaCl solution was sequential from the smallest to the highest concentration, but it was ensured that it was fully saturated (2 pore volumes of each fluid were produced) before the data acquisition. The results of zeta potential and streaming potential coefficient for each electrolyte solution of NaCl are given in Table D.1.

Table D.1. Experimental values of experiments with NaCl solutions in Fontana blue.

NaCl flooding in Fontainebleau SST		
Concentration (ppm)	**ζ (V)**	***Cs* (V/Pa)**
500	-0.07317	1×10^{-7}
1000	-0.08645	6×10^{-8}
5000	-0.06283	1×10^{-8}
10000	-0.0617	5×10^{-9}

Appendix E

Henry's law for equilibrium fluids

William Henry studied the solubility of gases in aqua solutions. Based on his experimental results, in 1803 he developed a formula to describe this phenomenon. This formula yields:

$$H^{cp} = c_a/p \quad \text{(E-1)}$$

Where, H^{cp} refers to Henry's solubility; c_a is the concentration of spices; and p is the partial pressure.

According to the publication of Carroll et al. [53] in 1992, for a CO_2-H_2O system, Henry's constant can be estimated accurately within the temperature range of 0-100 °C by the model of Krichevsky-Kasarnovsky (KK), which is provided in Figure E.1. The KK equation is given as:

$$p_{CO_2} = H' \, x_{co_2} \quad \text{(E-2)}$$

where, p_{CO2} is the partial pressure and x_{CO2} refers to the equilibrium mole fraction. Note that the above equation operates under the assumption that *CO2* is a single simple gas.

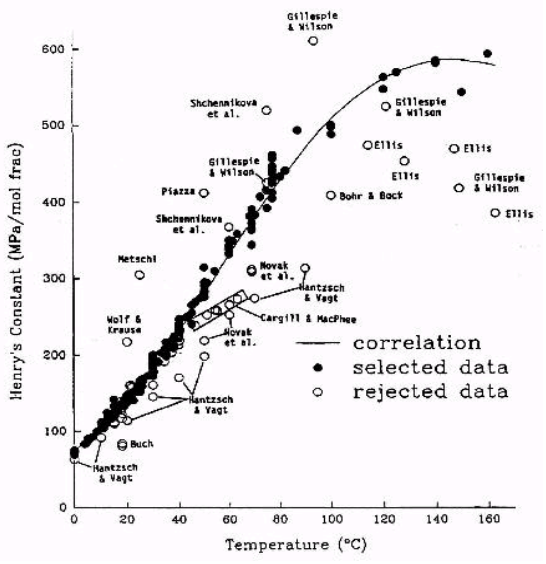

Figure E.1. Henry's coefficient of CO_2 dissolution in water. The picture adapted from Carroll et al. [53].

Appendix F

Equilibrium carbonic species formulation

The equations of equilibrium carbonic species, discussed previously, have been obtained from the publication of Mook et al. [55] in 2000. Despite that, we have presented the derivations according to their publications, the details that are not related with our research are excluded and thus we highly recommend this source as a reference for further information.

The concentration of all the equilibrium carbonic species or total inorganic concentration (c_{tot}) can be written as:

$$c_{tot} = [HCO_3^- + H_2CO_3 + CO_3^{2-}] \quad \text{(F-1)}$$

In addition the two dissociation constants can be defined as:

$$K_1 = \frac{[H^+][HCO_3^-]}{[H_2CO_3]} \quad \text{(F-2)}$$

$$K_2 = \frac{[H^+][CO_3^{2-}]}{[HCO_3^-]} \quad \text{(F-3)}$$

By rearranging the terms of the equation F-2and F-3 we obtain:

$$[H_2CO_3] = \frac{[H^+]}{K_1}[HCO_3^-] \quad \text{(F-4)}$$

$$[CO_3^{2-}] = \frac{K_2}{[H^+]}[HCO_3^-] \quad \text{(F-5)}$$

The distribution of the concentrations for each carbonic specie can be derived by solving equation F-1 with respect to equation F-4 and F-5 such as:

$$c_{tot} = \left[1 + \frac{K_2}{[H^+]} + \frac{[H^+]}{K_1}\right][HCO_3^-] \quad \text{(F-6)}$$

$$c_{tot} = \left[\frac{[H^+]}{K_2} + \frac{[H^+]^2}{K_1K_2} + 1\right][CO_3^{2-}] \quad \text{(F-7)}$$

$$c_{tot} = \left[\frac{K_1}{[H^+]} + 1 + \frac{K_1K_2}{[H^+]^2}\right][H_2CO_3] \quad \text{(F-8)}$$

References

[1] Jacob H. Masliyah and Subir Bhattacharjee. *Electrokinetic and colloid transport phenomena.* John Wiley & Sons, 2006.

[2] Robert J. Hhunter. *Zeta potential in colloid science*. 1981.

[3] B. Suski, F. Ladner, L. Baron, F. D. Vuataz, F. Philippossian, and K. Holliger. *Detection and characterization of hydraulically active fractures in a carbonate aquifer: results from self-potential, temperature and fluid electrical conductivity logging in the combioula hydrothermal system in the southwestern swiss alps*. Hydrogeology Journal, 16(7):1319–1328, 2008.

[4] A. Revil, P.A. Pezard, and P.W.J. *Glover. Streaming potential in porous media: 1. theory of the zeta potential.* Journal of Geophysical Research: Solid Earth, 104(B9):20021– 20031, 1999.

[5] Mathieu Darnet and Guy Marquis. *Modelling streaming potential (SP) signals induced by water movement in the vadose zone*. Journal of hydrology, 285(1):114–124, 2004.

[6] Jon H. Saunders, Matthew D. Jackson, and Christopher C. Pain. *Fluid flow monitoring in oil fields using downhole measurements of electrokinetic potential*. Geophysics, 73(5):E165–E180, 2008.

[7] Alex Goh. *Controlled salinity waterflooding in carbonates: Evidence, mechanisms, and comparative study with sandstones.* 2014.

[8] Steve R. Pride and F. D. Morgan. *Electrokinetic dissipation induced by seismic waves*. Geophysics, 56(7):914–925, 1991.

[9] J.H. Saunders, M.D. Jackson, and C.C. Pain. *A new numeri-cal model of electrokinetic potential response during hy-drocarbon recovery*. Geophysical research letters, 33(15), 2006.

[10] Anthony Szymczyk, André Pierre, Jean Claude Reggiani, and Jacques Pagetti. *Characterisation of the electrokinetic properties of plane inorganic membranes using streaming potential measurements*. Journal of membrane science, 134(1):59–66, 1997.

[11] Paul W. Glover and Nicholas Déry. *Streaming potential coupling coefficient of quartz glass bead packs: Dependence on grain diameter, pore size, and pore throat radius*. Geophysics, 75(6):F225–F241, 2010.

[12] F. D. Morgan, E. R. Williams, and T. R. Madden. *Streaming potential properties of westerly granite with applications*. Journal of Geophysical Research: Solid Earth, 94(B9):12449–12461, 1989.

[13] David Linton Johnson, Joel Koplik, and Roger Dashen. *Theory of dynamic permeability and tortuosity in fluid-saturated porous media*. Journal of fluid mechanics, 176(1):379–402, 1987.

[14] Paul W. J. Glover, Emilie Walker, and Matthew D. Jackson. *Streaming-potential coefficient of reservoir rock: A theoretical model*. Geophysics, 77(2):D17–D43, 2012.

[15] Carsten Werner, Ralf Zimmermann, and Thomas Kratzmüller. *Streaming potential and streaming current measurements at planar solid/liquid interfaces for simultaneous determination of zeta potential and surface*

conductivity. Colloids and Surfaces A: Physicochemical and Engineering Aspects, 192(1):205–213, 2001.

[16] Laurier L. Schramm, Karin Mannhardt, and Jerry J. Novosad. *Electrokinetic properties of reservoir rock particles*. Colloids and surfaces, 55:309–331, 1991.

[17] Mehran Sohrabi, Masoud Riazi, Mahmoud Jamiolahmady, Nor Idah Kechut, Shaun Ireland, and Graeme Robertson. *Carbonated water injection (CWI) – a productive way of using CO_2 for oil recovery and CO_2 storage*. Energy Procedia, 4:2192–2199, 2011.

[18] Jalal Foroozesh, Mahmoud Jamiolahmady, Mehran Sedah Sohrabi, and Shaun Ireland. *Mathematical modelling of carbonated water injection including mass transfer kinetics*, volume 2, pages 1052–1058. Society of Petroleum Engineers, 9 2013.

[19] Mehran Sohrabi, Masoud Riazi, Mahmoud Jamiolahmady, Shaun Ireland, and Chris Brown. *Mechanisms of oil recovery by carbonated water injection.* In SCA annual meeting, 2009.

[20] Jalal Foroozesh, Mahmoud Jamiolahmady, and Mehran Sohrabi. *Mathematical modeling of carbonated water injection for EOR and CO_2 storage with a focus on mass transfer kinetics*. Fuel, 174:325–332, 2016.

[21] J. MIJTTERLOSE and A. STADTLER. *Characterization of a shallow marine sandstone reservoir in a syn—rift setting: The Bentheim sandstone formation (valanginian) of the Ruhlermoor field, lower Saxony basin, NW Germany.*

[22] Jörg Mutterlose and André Bornemann. *Distribution and facies patterns of lower cretaceous sediments in northern Germany: a review*. Cretaceous Research, 21(6):733–759, 2000.

[23] Médard Thiry. *Weathering morphologies of the Fontainebleau sandstone and related silica mobility*. Ferrantia, 44:47–51, 2005.

[24] M. R. Cooper, J. Evans, S. S. Flint, A. J. C. Hogg, and R. H. Hunter. *Quantification of detrital, authigenic and porosity components of the Fontainebleau sandstone: A comparison of conventional optical and combined scanning electron microscope-based methods of modal analyses. Quartz Cementation in Sandstones*, pages 89–101, 2009.

[25] B. Rousset-Tournier, F. Mazerolle, Y. Géraud, and D. Jeannette. *Rock drying tests monitored by x-ray computed tomography—the effect of saturation methods on drying behaviour*. Geological Society, London, Special Publications, 215(1):117–125, 2003.

[26] Thierry Bourbie and Bernard Zinszner. *Hydraulic and acoustic properties as a function of porosity in Fontainebleau sandstone.* Journal of Geophysical Research: Solid Earth, 90(B13):11524–11532, 1985.

[27] David A. Coker, Salvatore Torquato, and John H. Dunsmuir. *Morphology and physical properties of Fontainebleau sandstone via a tomographic analysis.* JOURNAL OF GEOPHYSICAL RESEARCH-ALL SERIES

[28] Ibrahim Mohamed Mohamed, Jia He, Hisham A. Nasr-El-Din, et al. *Permeability change during CO_2 injection in carbonate rock: A coreflood study*. In SPE Produc-tion and Operations Symposium. Society of Petroleum Engineers, 2011.

[29] S. L. Phillips, H. Ozbek, and R. J. Otto. *Basic energy properties of electrolytic solutions database*: paper presented at sixth international codata conference, 2–25, 1978.

[30] Steve Pride. *Governing equations for the coupled electromagnetics and acoustics of porous media*. Physical Review B, 50(21):15678, 1994.

[31] Andrew James McMahon, K. Blakley, et al. *The controversy of CO_2 solubility in water.* In CORROSION 98. NACE International, 1998.

[32] Frank J. Millero, Denis Pierrot, Kitack Lee, Rik Wanninkhof, Richard Feely, Christopher L. Sabine, Robert M. Key, and Taro Takahashi. *Dissociation constants for carbonic acid determined from field measurements.* Deep Sea Research Part I: Oceanographic Research Papers, 49(10):1705–1723, 2002.

[33] Pabitra N. Sen and Peter A. Goode. *Influence of temperature on electrical conductivity on shaly sands*. Geophysics, 57(1):89–96, 1992.

[34] Truman S. Light, B. Kingman, and Anthony C. Bevilacqua. *The conductivity of low concentrations of CO_2 dissolved in ultrapure water from 0-100 °C*. In 209th American Chemical Society National Meeting, pages 2–6, 1995.

[35] G. Lefevre, M. Duc, and M. Fedoroff. *Effect of solubility on the determination of the protonable surface site density of oxyhydroxides*. Journal of colloid and interface science, 269(2):274–282, 2004.

[36] Sven H. Behrens and David G. Grier. *The charge of glass and silica surfaces*. The Journal of Chemical Physics, 115(14):6716–6721, 2001.

[37] Stephen Lofts and Edward Tipping*. An assemblage model for cation binding by natural particulate matter*.

Geochimica et Cosmochimica Acta, 62(15):2609–2625, 1998.

[38] Ward Chesworth et al. *Encyclopedia of soil science*, volume 207. Springer, 2008.

[39] Espen S. Hamborg, John P. M. Niederer, and Geert F. Versteeg. *Dissociation constants and thermodynamic properties of amino acids used in CO_2 absorption from (293 to 353) K*. Journal of Chemical & Engineering Data,

52(6):2491–2502, 2007.

[40] Yiteng Su, Lihong Peng, Angus Shiue, Gui-Bing Hong, Zhang Qian, and Chang-Tang Chang. *Carbon dioxide adsorption on amine-impregnated mesoporous materials prepared from spent quartz sand*. Journal of the Air & Waste Management Association, 64(7):827–833, 2014.

[41] JO Leckie. *Characterization of surface processes on mineral surfaces in aqueous solutions*. Annual report for fiscal year 1993. Technical report, Los Alamos National Lab., NM (United States); Stanford Univ., CA (United States). Dept. of Civil Engineering, 1993.

[42] Shuai Li, Philippe Leroy, Frank Heberling, Nicolas Devau, Damien Jougnot, and Christophe Chiaberge. *Influence of surface conductivity on the apparent zeta potential of calcite*. Journal of colloid and interface science, 468:262–275, 2016.

[43] André Watillon and Roland De Backer. *Potentiel d'écoulement, courant d'écoulement et conductance de surface à l'interface eau-verre*. Journal of Electroanalytical Chemistry and Interfacial Electrochemistry, 25(2):181–196, 1970.

[44] Syed Muhammad Al-Amsyar. *Porous silica materials-polymer composite as proton Conducting membrane for fuel cell*. PhD thesis, Faculty of Science, 2007.

[45] Michal Borkovec, Sven H Behrens, and Micha Semmler. *Observation of the mobility maximum predicted by the standard electrokinetic model for highly charged amidine latex particles*. Langmuir, 16(11):5209–5212, 2000.

[46] A. Revil and P. W. J. Glover. *Nature of surface electrical conductivity in natural sands, sandstones, and clays*. Geophysical Research Letters, 25(5):691–694, 1998.

[47] DT Luong et al. *Electrokinetics in porous media*. 2014.

[48] F. Scholz. *Electroanalytical methods: guide to experiments and applications*. 2002, 1995.

[49] R. M. De Velde Harsenhorst. *Electrokinetics in Low Salinity Waterflooding*. PhD thesis, TU Delft, Delft University of Technology, 2014.

[50] Phil Attard. *Electrolytes and the electric double layer*. Advances in Chemical Physics, 92:1–160, 1996.

[51] Hainan Wang and Laurent Pilon. *Accurate simulations of electric double layer capacitance of ultramicroelectrodes*. The Journal of Physical Chemistry C, 115(33):16711–16719, 2011.

[52] Hilmi S. Salem. *Determination of porosity, formation resistivity factor, Archie cementation factor, and pore geometry factor for a glacial aquifer*. Energy sources, 23(6):589–596, 2001.

[53] Carroll, John J., and Alan E. Mather. *The system carbon dioxide-water and the Krichevsky-Kasarnovsky equation*. *Journal of Solution Chemistry* 21.7 (1992): 607-621.

[54] Rechard, E. Z., and W. Dieter. *CO_2 in Seawater: Equilibrium, Kinetics, Isotopes*. Elsevier oceanography series 65 (2003).

[55] Mook, Willem G., and J. J. De Vries. *Volume I: Introduction: Theory, Methods, Review*. Environmental Isotopes in the Hydrological Cycle—Principles and Applications, International Hydrological Programme (IHP-V), Technical Documents in Hydrology (IAEA/UNESCO) No 39 (2000): 75-76.

[56] Yakushev, Evgeniy, and Kai Sørensen. *Ocean acidification and carbonate system parameters measurements*. (2010).

[57] Jaafar, M. Z., J. Vinogradov, and M. D. Jackson. *Measurement of streaming potential coupling coefficient in sandstones saturated with high salinity NaCl brine*. *Geophysical Research Letters* 36.21 (2009).

[58] Vinogradov, J., M. Z. Jaafar, and M. D. Jackson. *Measurement of streaming potential coupling coefficient in sandstones saturated with natural and artificial brines at high salinity.* Journal of Geophysical Research: Solid Earth 115.B12 (2010).

LIST OF ABBREVATIONS

CW	Darbonated water
DM	Demineralized water
DG	Degassed water
HS	Helmholtz and Smoluchowski
EDL	Electrical double layer
SST	Sandstone

LIST OF SYMBOLS

c_{tot}	(mol/l)	Equilibrium mole fraction in liquid phase
d	(m)	Grain
e	(mol^{-1})	Charge of an electrode
k	(mD)	Permeability
k_b	(J/K)	Boltzmann's constant
m	(-)	Cementation factor
n	(-)	Number of moles
p	(Pa)	Partial pressure
r	(m)	Grain radius
x_{co2}	(-)	Equilibrium mole fraction
zi	(-)	Number of ionic species
A	(g/mol)	Atomic mass of carbon dioxide
C_α	(mol/l)	Concentration of acid
C_b	(mol/l)	Concentration of base
C_f	(mol/l)	Fuild concentration
C_f^m	(mol/l)	Molarity
C_i^f	(mol/l)	Concentration of a single ionic specie
F	(-)	Formation factor
H'	(Pa)	Henry's constant
I_f	(mol/l)	Ionic strength
K_	(-)	Disassociation constant For dehydrogenization of silanol
K_{me}	(-)	Binding constant for cation adsorption of quartz
K_w	(-)	Dissociation constant
K_1	(-)	Equilibrium dissociation constant of CO_2 in water
K_2	(-)	Equilibrium dissociation constant of carbonate ion in water
N	(F/m)	Avogadro's number
P	(Pa)	Pressure
Q	(ml/min)	Flow rate
R	(J/mol.K)	Ideal gas constant
R_b	(Ω)	Resistivity of saturated formation
R_o	(Ω)	Resistivity of water
R_t	(Ω)	Resistivity of a rock at irreducible water saturation
R_w	(Ω)	Resistivity of water at formation temperature
T	(K), (°C)	Temperature
V	(l)	Volume
β_s	(m^2/sV)	Surface ionic mobility
ε_f	(F/M)	Fluid electrical permittivity
ε_o	(F/m)	Dielectric permittivity in vacuo
ε_r	(-)	Fluid relative electrical permittivity
ζ	(V)	Zeta potential
ζ_0	(V)	Zeta zero offset
η_f	(Pa.s)	Fluid dynamic viscosity
ρ_f	(g/cm^3)	Fluid density
σ_f	(S/m)	Fluid conductivity
φ	(-)	Porosity
φ_d	(V)	Stern plane potential
χ	(m)	Distance of potential from the mineral surface
χ_d	(m)	Debye length
χ_ζ	(m)	Stern plane distance
Γ_s	(site/m^2)	Surface site density
ΔP	(Pa)	Pressure difference
ΔV	(V)	Voltage difference
Λ	(m)	Length scale of pore microstructure
Σ_s	(S)	Surface conduction
Σ_s^{EDL}	(S)	Electrical double layer conduction
Σ_s^{prot}	(S)	Proton conduction
Σ_s^{stern}	(S)	Stern layer conduction